ISTANBUL TECHNICAL UNIVERSITY ★ GRADUATE SCHOOL OF SCIENCE ENGINEERING AND TECHNOLOGY

NUMERICAL MODELLING OF EARTHQUAKE-INDUCED SEABED LIQUEFACTION

M.Sc. THESIS

Giray ÇIVAK

Department of Coastal Sciences and Engineering

Coastal Sciences and Engineering Programme

JUNE 2019

ISTANBUL TECHNICAL UNIVERSITY ★ GRADUATE SCHOOL OF SCIENCE ENGINEERING AND TECHNOLOGY

NUMERICAL MODELLING OF EARTHQUAKE-INDUCED SEABED LIQUEFACTION

M.Sc. THESIS

Giray ÇIVAK
(517141001)

Department of Coastal Sciences and Engineering

Coastal Sciences and Engineering Programme

Thesis Advisor: Assoc. Prof. Dr. V. Ş. Özgür KIRCA

JUNE 2019

İSTANBUL TEKNİK ÜNİVERSİTESİ ★ FEN BİLİMLERİ ENSTİTÜSÜ

DENİZ TABANINDA DEPREM KAYNAKLI SIVILAŞMANIN SAYISAL OLARAK MODELLENMESİ

YÜKSEK LİSANS TEZİ

Giray ÇIVAK
(517141001)

Kıyı Bilimleri ve Mühendisliği Ana Bilim Dalı

Kıyı Bilimleri ve Mühendisliği Programı

Tez Danışmanı: Doç. Dr. V.Ş. Özgür KIRCA

HAZİRAN 2019

Giray ÇIVAK, a M.Sc. student of ITU Graduate School of Science Engineering and Technology 517141001 successfully defended the thesis entitled "NUMERICAL MODELLING OF EARTHQUAKE-INDUCED SEABED LIQUEFACTION", which he/she prepared after fulfilling the requirements specified in the associated legislations, before the jury whose signatures are below.

Thesis Advisor :	**Assoc. Prof. Dr. V. Ş. Özgür KIRCA** Istanbul Technical University	.....
Jury Members :	**Prof. Dr. Şevket ÇOKGÖR** Istanbul Technical University	.....
	Assoc. Prof. Dr. Mehmet ÖZTÜRK Yıldız Technical University	.....
		.....

Date of Submission : **3 May 2019**
Date of Defense : **10 June 2019**

To my grandmother Mutia Çıvak,

FOREWORD

Since Alen Hazen first used the word “liquefies” for such soil failure in 1920, numerous soil failures have been reported in engineering literature in relation with the liquefaction phenomena. In this thesis, the adaptation of a numerical model which calculates pore water pressure under cyclic loading due to waves was done to predict earthquake-induced seabed liquefaction.

I would like to thank my supervisor Assoc. Prof. V.Ş. Özgür Kırca, who was the reason for me to choose to become a coastal engineer, for his precious trust and true guidance; Prof. M. Sedat Kabdaşlı, Atakan Yüce and CEC Marine family for all their trust and support starting from the early days of my career. In truth, I could not have achieved my current level in my short career without them. I would also like to thank Merih Özcan for his support for presenting a conference paper on this thesis. Finally, I am now and will always be grateful to my parents and my wife for their endless support.

June 2019

Giray ÇIVAK
(Civil Engineer)

TABLE OF CONTENTS

Page

ABBREVIATIONS

BPT : Becker Penetration Test
CPT : Cone Penetration Test
CRR : Cyclic Resistance Ratio
CSR : Cyclic Shear Ratio
ER : Hammer Energy Ratio
MSF : Magnitude Scalling Factor
SPT : Standard Penetration Test

SYMBOLS

$a(t)$	: Cyclic acceleration
C_E	: Correction factor for hammer energy ratio
C_B	: Correction factor for bore-hole diameter
C_N	: Correction factor for effective over-burden stress
C_R	: Correction factor for rod length
C_S	: Correction factor for sampling method
D_r	: Relative density of the soil
E	: Modulus of elasticity
τ	: Shear stress
τ_{max}	: Maximum shear stress
τ_a	: Average equivalent uniform shear stress
K	: Lateral earth pressure coefficient
K_σ	: High over-burden correction factor
K_α	: Static shear stress correction factor
g	: Acceleration of gravity
$\mathbf{N_x}$, $\mathbf{N_y}$, $\mathbf{N_z}$	: Normal Power Components
γ_t	: Specific total weight of soil
t	: Time
T	: Shaking period
r_d	: Stress reduction factor
h	: Water depth
k	: Hydraulic conductivity
ϕ'	: Angle of internal friction
V_s	: Shear wave velocity
$\bar{p}$	: Period averaged pressure value
σ_0	: Initial total stress
σ'_0	: Initial effective stress
I_D	: Density index
σ'_{v0}	: Initial vertical effective stress
S_r	: Degree of saturation
s	: Specific gravity
e_{max}	: Maximum void ratio
e_{min}	: Minimum void ratio
N_m	: Measured standard penetration resistance
$(N_1)_{60}$	: Corrected SPT blow count
N_m	: Measured standard penetration resistance
z	: Depth

LIST OF TABLES

Page

LIST OF FIGURES

Page

NUMERICAL MODELLING
OF
EARTHQUAKE-INDUCED SEABED LIQUEFACTION

SUMMARY

Under cyclic loading conditions, shear deformations gradually rearrange soil grains and the pore water pressure increases in saturated, undrained soils at the expense of pore volume. In case of the presence of sufficient time and room, the pore water pressure reaches such a level that exceeds initial effective stresses and because of disappearing stresses between individual grains, the soil acts like a fluid, loses the ability to bear any load thus it fails. The term "liquefaction" is used to define this phenomenon in engineering terminology. It has been recognized that soils that can be liquefied under cyclic conditions are basically limited to fine soils or composite soils such as silty or clayey sands. As it was mentioned in the definition, liquefaction susceptibility is closely related with sort of soil parameters and cyclic loading conditions as expected. Through the years many soil failures caused by earthquake induced liquefaction has been reported by engineers and scientists. For example; in 1999 Kocaeli earthquake, an extensive liquefaction caused sinking of breakwaters, large displacements of quay walls and huge settlements of back-fills which were resulted in serious damages to coastal structures. There are limited comprehensive analysis methods for earthquake induced seabed liquefaction and ordinarily, specially prepared charts where the dimensionless parameter Cyclic Stress Ratio (CSR) is plotted versus corrected SPT blow counts gathered from Standard Penetration Tests to define relative density of the soil have been used by practitioners to assess liquefaction susceptibility, albeit as a first approximation. Because of the incapability of obtaining undisturbed specimens to be analyzed in the laboratory, empirical approach based in-situ penetration test results gained more popularity among engineers, and therefore, SPT based assessments were referred to in this study. In this thesis; an experimentally-validated mathematical model (Sumer, *et. al.*, 2012), which was originally developed for wave induced liquefaction, was modified and adapted to predict earthquake-induced seabed liquefaction. While earthquakes and waves both produce cyclic shear stresses (and accordingly cyclic shear deformations) in the seabed, the ones induced by earthquakes are more severe compared to that caused by waves. The early results obtained from this modified mathematical model were compared to the widely used CSR-SPT assessments to investigate liquefaction susceptibility. The method used in this study basically covers the comparison of the results obtained from a series of parametric model runs with the estimated ones from recent CSR-SPT liquefaction susceptibility assessment procedures. Primarily, earthquake-soil interaction was analyzed, then the shear stresses caused by cyclic loading during an earthquake were used as the model input. A stress based equation is used with proper reduction coefficients to translate maximum cyclic ground acceleration during an earthquake into average equivalent cyclic shear stresses generated in the seabed. The modified one-dimensional mathematical model basically simulates the pore pressure build-up under cyclic loading conditions depending on

the intensity of shear stresses/deformations. Different cyclic loading conditions were done for various relative densities (D_r) in the model tests to compare results with the CSR-SPT assessments. First results showed that the adapted model could estimate earthquake-induced pore pressure build-up and seabed liquefaction, especially for soils have up to 30 or less SPT blow counts. Moreover, a calibration assessment was done to increase the estimation ability of the adapted model. Suggested correlations between Young's modulus of elasticity and corrected standard penetration blow counts were evaluated to calibrate model. After comparison with the reference cyclic resistance ratio curve, model results were also compared with the recent liquefaction site data. It was seen that the calibrated model has a satisfactory ability to predict earthquake-induced seabed liquefaction. Investigation of the adapted models capabilities was done by conducted a series of parametric model runs and the results were discussed.

DENİZ TABANINDA DEPREM KAYNAKLI SIVILAŞMANIN SAYISAL OLARAK MODELLENMESİ

ÖZET

Bu çalışma kapsamında; dalga kaynaklı deniz tabanı sıvılaşması için kullanılagelen ve deneysel verilere karşı doğrulanmış bir matematik model, deprem kaynaklı deniz tabanı sıvılaşması modellenmesi için geliştirilerek uyarlanmıştır.

Hem dalga etkisi hem de deprem etkisi deniz tabanı üzerinde tekrarlı kayma gerilmelerine bağlı olarak tekrarlı kayma deformasyonları yaratmakta ve deniz tabanının sıvılaşmasına yol açabilmektedir. Çalışma içeriğinde yer alan söz konusu tek boyutlu matematik model vasıtasıyla, deniz tabanı zemininde deprem kaynaklı tekrarlı yükler altındaki boşluk suyu basıncının gelişimi ve davranışı benzeştirilerek, deniz tabanının deprem etkisi altındaki sıvılaşma süreci incelenmiştir.

Zemin danelerinin tekrarlı yükleme altında gösterdikleri yeniden yerleşme eğilimi, zamanla zeminin içerisindeki efektif gerilmelerin azalmasına ve mevcut boşluk suyu basıncının artmasına neden olmaktadır. Boşluk suyu basıncının zemin efektif gerilmelerinden fazla olduğu anda ise zemin bir akışkan gibi davranmaya başlar ve taşıyıcılığını yitirir. Bu durum "zemin sıvılaşması" olarak tanımlanmaktadır. Genel olarak, ince daneli veya silt ve kil muhteviyatlı kompozit zeminler tekrarlı yükleme koşulları altında sıvılaşabilecek zeminler olarak kabul edilirler. Sıvılaşma süreci zemin daneleri arasındaki bağ tekrar oluşuncaya ve boşluk suyu tahliye yetisi kazanıncaya dek devam eder. Tanımında yer aldığı üzere; zeminin sıvılaşma potansiyeli, bahsedilen süreçler göz önüne alındığında, tekrarlı yükleme koşulları ve zemin fiziksel parametreleri ile yakından ilgilidir.

Doğada tekrarlı yükleme koşulları depremler benzeri sismik faaliyetler sonucu sıklıkla görüldüğünden, deprem etkisinde terarlı yüklemeler maruz kalan zeminlerin sıvılaşarak taşıyıcılıklarını yitirdikleri vakalar literatürde sıkça yer bulmuştur. Örnek olarak 1999'da yaşanan Kocaeli Depremi sonrasında, depremde meydana gelen zemin sıvılaşmasına bağlı batmış dalgakıranlar, rıhtım duvarları gibi ağırlık yapılarında yer değiştirmeler ve benzer kıyı yapılarında ciddi oturmalar rapor edilmiştir (Sumer ve diğ., 2007). Bütün bu hasarlardan mühendisliğin ilgili alanlarının istifade edebileceği önemli bulgular tecrübe edilmiştir. Deprem kaynaklı deniz tabanı sıvılaşması ile ilgili ayrıntılı analiz yöntemleri kısıtlı olup, uygulamada öncelikli yaklaşım olarak sıkça kullanılan yöntem; tekrarlı gerilme oranlarına (Cyclic Stress Ratio, CSR) karşı çizdirilen düzeltilmiş SPT (Standart Penetrasyon Testi) darbe sayıları grafiklerini kullanmaktır. Boyutsuz parametreler üzerinden kontrol imkanı sunan abaklar uygulamacılar tarafından sıklıkla tercih edilmekte, ancak yalnız bir ön teşhis (preliminary screening) imkanı sunmaktadırlar. Bu çalışmada, dalga kaynaklı deniz tabanı sıvılaşması için kullanılagelen ve deneysel verilere karşı doğrulanmış bir matematik model (Sumer ve diğ., 2012), deprem kaynaklı deniz tabanı sıvılaşması modellenmesi için geliştirilerek uyarlanmıştır.

Çalışmada kullanılan yöntem, deneysel olarak doğrulanmış bir dalga kaynaklı zemin sıvılaşma modelinin deprem kaynaklı zemin sıvılaşması potansiyelini belirlemek üzere

uyarlanmasını esas alır. Değiştirilip uyarlanan bu tek boyutlu modelin, bir dizi parametrik koşumu neticesinde elde edilen sonuçlar temel CSR-SPT (N) grafikleri ile karşılaştırılarak değerlendirilmiştir. Bu kapsamda öncelikli olarak, deprem-zemin etkileşimi irdelenerek deprem esnasında meydana gelen tekrarlı yüklemelere bağlı kayma gerilmeleri model girdisi olarak kullanılmıştır.

Söz konusu kayma gerilmeleri zeminde kayma deformasyonları yaratacak ve sürecin devamında, eğer uygun koşulların varlığı söz konusu ise, boşluk suyu basınçlanarak "sıvılaşma" meydana gelecektir. Diğer yandan tekrarlı yüklemenin şiddeti ve süresi de sıvılaşmanın oluşabilmesi için belirleyicidir. Zemin ivmeleri ve kayma gerilmeleri arasındaki ilişki açıklanırken temel yaklaşım yukarıda şematize edildiği üzere zemin kolonunun rijit cisim davranışında bulunduğu kabulüdür. Ancak zemin gerçekte biçim değiştirebilen (deforme olabilen) bir yapıya sahip olduğundan, "z" derinliğinde zeminin maruz kalacağı maksimum kayma gerilmesi rijit cisim kabulünü içeren yaklaşımda ifade edilen kayma gerilmelerinden daha az olacaktır. Bu durumda ilgili eşitliğe derinliğe bağlı olarak verilen bir azaltma katsayısının (r_d) eklenmesi gerekecektir (Liao, 1986).

Deprem sırasında zemin kayma gerilmeleri düzensiz bir zaman serisi oluşturmaktadır. Bu durum bir ortalama eşdeğer kayma gerilmesi τ_a tanımlanmasını gerektirmektedir. Ortalama eşdeğer kayma gerilmesi; Seed (1971) tarafından bir dizi test neticesinde kayda değer bir doğrulukla birlikte önerilen haliyle zemin kolonunun maruz kaldığı en büyük ivmenin 65%'i olacak şekilde değerlendirilmiştir.

Bu basitleştirilmiş yaklaşım aynı zamanda model sonuçlarıyla karşılaştırma yapılacak CSR yönteminde de aynen uygulanmaktadır. Bu yöntemde, ilgili eşitlik kullanılarak hesap edilen CSR değeri, referans alınan zemin tipi ve deprem büyüklüğüne ait tekrarlı direnç oranı (Cyclic Resistance Ratio) ile oranlanarak bir güvenlik katsayısı (FS) elde edilir. Bu güvenlik katsayısı ise, belirli büyüklükteki depremlerin meydana geldiği sırada ilgi alanındaki zeminde oluşabilecek sıvılaşmanın potansiyeli ile ilgili tahminde bulunulmasına imkan verir.

Deprem sırasında bir zeminin sıvılaşma potansiyelini belirleyebilmek için elbette bir takım farklı zemin parametrelerine de ihtiyaç duyulmaktadır. Zeminlerin sıvılaşma potansiyelini belirleyebilmek için başvurulan detaylı bir diğer yöntem ise araştırılacak zemine ait tekrarlı gerilme laboratuvar testleri veya santrifüj sarsma tablası testlerinin teşkil edilmesidir. Ancak bu testler zor ve pahalı olduğu kadar, testlerin sağlıklı ve verimli bir şekilde uygulanabilmesi için ihtiyaç duyulan örselenmemiş numunelerin temini oldukça zordur. Bu sebeple sahada uygulanan ve güvenilir kabul edilen "Standart Penetrasyon Testleri" neticesinde elde edilen verilere başvurmak en pratik alternatif olarak ortaya çıkmaktadır. Standart penetrasyon testi yaygın olarak kullanılan ve yerinde ölçme imkanı veren bir zemin deneyidir. Test basitçe, zemin direncinin bir referans yöntem ve penetrasyon aleti kullanılarak tahmin edilmesini sağlamaktadır. Bu testlere ait darbe sayılarından oluşan sonuçlar ise ilgi zeminin sıkılığına (D_r) dair fikir vermeleri açısından bu çalışmada esas alınmıştır. Zira standart CSR abaklarında da benzer bir yaklaşım söz konusudur.

Çalışmada kullanılan SPT-N değerlerine karşılık gelen zemin sıkılıkları; Powrie, 2013'te verilen tablolar kullanılarak elde edilmiştir. Modellenen zemin tiplerine ait sıkılıklar bu tabloda yer alan veriler kullanılarak, ihtiyaç duyulan aralık değerlerini belirlemek için ise gerektiğinde 3. dereceden polinom interpolasyonu uygulanarak elde edilmiştir.

Çalışmada kullanılan model, esasen dalga kaynaklı zemin sıvılaşmasını modellemek için geliştirilmiş ve deneysel olarak doğrulanmış bir modeldir (Sumer ve diğ. , 2012).

Bu matematik modelde, boşluk suyu basıncı artışı Biot denklemlerinin tek boyutlu hali için bir difüzyon denklemine dönüşmektedir. Sonlu derinliğe sahip bir zemin kolonuna ait sınır ve başlangıç koşulları için denklemin çözümü ilk kez Sumer ve Fredsoe (2002) tarafından yapılmıştır.
Sonlu derinlikteki bir zemin kolonunun dalga kaynaklı sıvılaşması için başlangıç ve sınır koşulları belirlenerek bir çözüm yapılmıştır (Sumer ve Fredsoe, 2002). Bu çözüm, çalışmada kullanılan modelin temelini oluşturmaktadır. Modelin deprem kaynaklı zemin sıvılaşmasına uyarlanması ise, çözüm içinde ilerleyen dalgaların etkisi gözetilerek tanımlanan kayma gerilmesi teriminin, yukarıda bahsedilen biçimde deprem sırasında bir zemin kolonuna etkiyen gerilmelerle yeniden ifadesi ile gerçekleştirilmiştir.
Söz konusu modelin deprem etkisi altındaki deniz tabanı sıvılaşmasının potansiyelini tahmin etmedeki yetisi irdelenmiş ve elde edilen sonuçların pratikte yaygın kullanılan CSR metodu ile örtüşen neticeler verdiği gözlenmiştir.
Uyarlanan modelin kalibrasyonu ve doğrulanması CSR/CRR yaklaşımı ile elde edilen sonuçların karşılaştırılması ile yapılmıştır. Buna göre elde edilen ilk sonuçlar düşük zemin sıkılığı değerleri için doğru sonuçlar vermiş olsa da, modelin yüksek sıkılıktaki (30 ya da daha fazla düzeltilmiş SPT-N değerine sahip zeminler) zeminleri temsiliyeti değerlendirildiğinde kalibrasyona ihtiyaç duyduğu görülmüş ve model baz parametreleri irdelenmiştir. Modellerde kullanılan zemin parametreleri incelendiğinde, düşük ve yüksek sıkılığa sahip tüm zeminlerin aynı elastisite modülü değerine sahip olduğu görülmüştür. Bu aşamada orijinal modelin hassasiyeti ile ilgili literatür incelenmiş ve zemin sıkılığı ile elastisite modülü arasında bir korelasyon kullanılmasına karar verilmiştir. Zemin sıkılığı arttıkça, elastisite modülünü (E) arttırmak, yüksek sıkılıktaki zeminlerin modellendiği senaryolar için daha doğru ve mevcut sıvılaşma analizi yapılan yöntemlerin sonuçları ile örtüşen sonuçlar vermiştir.
Bir diğer adımda model sonuçları olasılık yöntemleri kullanılarak geliştirilen güncel deterministik zemin sıvılaşma tahmin metodları ile karşılaştırılmıştır. 200'den fazla saha kaydı, bu aşamada model kalibrasyonu için değerlendirilmiş ve modelin deprem kaynaklı zemin sıvılaşmasını tahmin etmedeki yeterliliği tatmin edici görülmüştür.
Kalibrasyon çalışmalarının ardından farklı zemin sıkılıkları (D_r), hidrolik iletkenlik değerleri (k), sıvılaşabilir zemin tabakası kalınlıkları (d), tekrarlı yükleme periyotları (T) ve içsel sürtünme açıları (ϕ) için parametrik karşılaştırmalar yapabilmem için model çalıştırılmıştır. Sonuçlar modelin, zemin sıvılaşması süreçlerinde etkinliği görülen parametrelerin sözkonusu etkilerini benzeştirmede yeterli olduğunu göstermektedir.

1. INTRODUCTION

Under cyclic loading conditions, shear deformations gradually rearrange soil grains and pore water pressure increases in saturated, undrained soils. If there is enough room and time, the pore water pressure reaches such a level that exceeds initial effective stresses and as a result of disappearing stresses between individual grains, the soil acts like a fluid, loses the ability to bear any load thus it fails. The term "liquefaction" is used to define this phenomenon in engineering terminology. It has been recognized that soils that can be liquefied under cyclic loading conditions are basically limited to fine soils or composite soils such as silty or clayey sands. Liquefaction process continues until the contact between soil particles is restored and pore water becomes able to drain again. Below figure (Figure 1.1) schematize liquefaction mechanism basically in three stages.

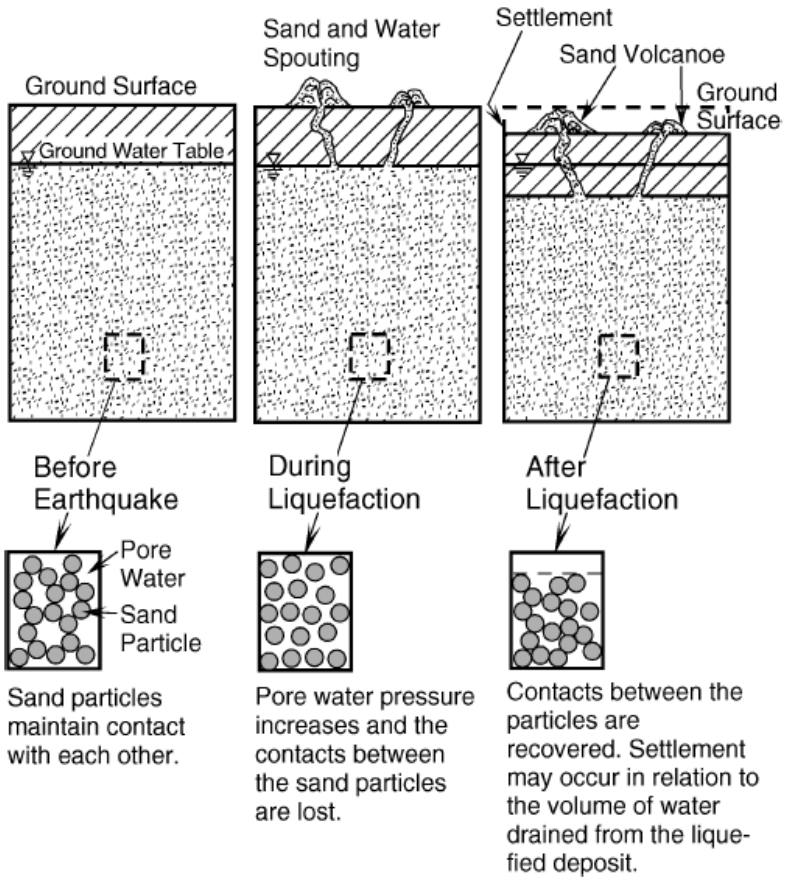

Figure 1.1 : Liquefaction mechanism [1].

Through the years, many soil failures caused by liquefaction has been reported by engineers and scientists. For example; in 1920, Allen Hazen -an hydraulics expert- first used the word “liquefies” in relation to such soil flow after the Calaveras Dam failure and in 1948, an earthquake in Fukui (Japan) caused alluvial soil liquefaction. In 1960, a pipeline flotation accident occurred near Fao Island in Shatt Al Arab delta due to waves and tidal motion. Beside, an earthquake in Niigata (a Japanese city which had been rebuilt after a huge fire in 1955) destroyed nearly all modern infrastructures due to soil liquefaction (Figure 1.3) and while in another case happened in the same year of 1964 in Alaska, a great earthquake of magnitude 9.2 caused huge landslides due to soil liquefaction. In 1969, Hurricane “Camille” caused wave-induced liquefaction and destroyed two marine structures. Furthermore, when Hyogoken-Nambu earthquake (a.k.a. Kobe earthquake, 1995) hit Kobe and Osaka regions in Japan, an extensive liquefaction caused damage to geotechnical structures just like liquefaction made damages to coastal structures (sinking of breakwaters, large displacements of quay walls, huge settlements of back fills etc.) in Kocaeli earthquake, 1999 [2–4].

Figure 1.2 : Tilting of apartment buildings after Niigata (Japan) earthquake in 1964 [3].

Researchers started investigations to assess liquefaction susceptibility after two catastrophic events occurred in 1964, Niigata and Alaska earthquakes.These two major events produced destructive effects related to soil liquefaction since then significant

Figure 1.3 : Floating of a buried tank after Niigata (Japan) earthquake in 1964 [3].

efforts to understand the liquefaction phenomenon have been made.

Apart from given examples above there are various reported examples of liquefaction failures in marine engineering literature. Flotation is just one of the possible failures of the seabed liquefaction as far as pipelines are concerned. A pipeline lighter than the soil may float through the seabed surface during liquefaction and could become exposed to any sort of external forces. Flotation of pipelines due to liquefaction of seabed caused by storms [5, 6] and subsidence of offshore breakwaters [7] have been subjected in notable researches.Sumer (2007) stated that "Liquefaction in the marine (or otherwise) environment occurs, not only, by waves or earthquakes but also by other effects as well" (p. 11). Other effects that cause soil liquefaction are expressed in the literature as shocks, blasts [8], solitary waves [9] and rocking motions that structures execute under cyclic loading.

1.1 Purpose of the thesis

While earthquakes and waves both produce cyclic shear stresses (and accordingly cyclic shear deformations) in the seabed, the ones induced by earthquakes are more severe compared to that caused by waves. There are limited comprehensive analysis methods for earthquake induced seabed liquefaction and ordinarily, specially prepared charts where the dimensionless parameter Cyclic Stress Ratio (CSR) is plotted versus

corrected SPT blow counts gathered from Standard Penetration Tests to define relative density of the soil have been used by practitioners to assess liquefaction susceptibility, albeit as a first approximation. Purpose of this thesis is basically to predict earthquake-induced seabed liquefaction by modifying an experimentally-validated mathematical model [10]. The results obtained from this modified mathematical model were compared to the widely used CSR-SPT assessments to investigate liquefaction susceptibility.

2. BACKGROUND

In this chapter scope of the study will be detailed by explaining background approaches and reviewing recent and previous studies in the literature.

2.1 Earthquake Induced Liquefaction

As the years passed by after two major earthquakes in 1964, engineers and scientists have been involved into investigation of liquefaction while earthquakes were providing data and lessons. Area of investigating liquefaction includes sub-topics and the first pace in most engineering treatments of soil liquefaction starts with "assessment of the likelihood of *'triggering'* or initiation of soil liquefaction". Beside, key elements of soil liquefaction engineering continues with the assessment of post liquefaction strength and overall post liquefaction stability, the assessment of expected liquefaction induced deformations, the assessment of consequences of deformations and ends with the implementation (and evaluation) of engineered mitigation [11]. As a scope of this study and in relation with the purpose of this thesis, this first step of "liquefaction triggering assessments" will be discussed in this section through geotechnical engineering perspective.

As it was mentioned in the definition, liquefaction susceptibility is closely related with sort of soil properties as expected. The first step to get an idea about the liquefaction potential of a soil is basically to investigate grain size distribution, liquid limit and water content of the soil. The Chinese criteria have been widely used in the engineering practice for this purpose. These criteria have been modified and formulated in the literature [12] and as an example, one them is summarized in the Table 2.1 below [13].

In addition to given Chinese criterion for liquefaction assessment, there are also some attempts to determine liquefaction susceptibility of soils. For instance, criteria for liquefaction susceptibility of fine grain sediments [11] and criteria for differentiating between sand-like and clay-like sediment behavior [14] are proposed in significant studies.

Table 2.1 : Modified Chinese criteria [13].

	Liquid Limit <32%	Liquid Limit ≥ 32%
Clay Content(< 0.002mm)<10%	Susceptible	Further studies required considering plastic non-clay sized grains
Clay Content(< 0.002mm)≥10%	Further studies required considering plastic non-clay sized grains	Non-susceptible

As in-situ tests are widely used in geotechnical engineering, practitioners have been searching for methods to use sort of tests to assess the liquefaction potential of the soil. Following paragraphs will include the main approaches that make *in-situ* tests applicable for liquefaction assessments.

Earthquakes are manifested as ground shaking caused by the sudden release of Earth's crust [15]. While the released energy propagates through the ground, the soil encounters forceful cyclic accelerations. The equation of motion for the one dimensional soil column is given in Equation 2.1 where; g is the acceleration of gravity, γ_t is the total specific weight of the soil, z is the depth of the soil column and $a(t)$ is the cyclic accelerations [2]. Physics of earthquake induced liquefaction starts with this simple equation that is used to translate *cyclic ground accelerations* caused by earthquakes into *cyclic shear stresses* in the soil.

$$\tau(t) = \frac{1}{g}\gamma_t z a(t) \tag{2.1}$$

Forces on the one dimensional soil column and cyclic shear stress variation which a soil element is exposed to during an earthquake are shown in the Figures 2.1 and 2.2. This mentioned cyclic shear stress variation causes the soil to undergo cyclic deformations leading to pressure buildup and after some time "liquefaction" if the soil is undrained.

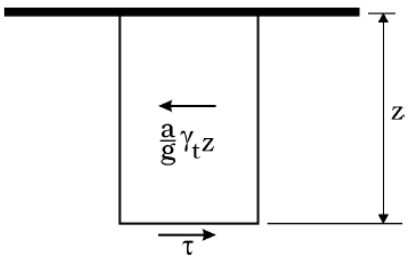

Figure 2.1 : Forces on the one dimensional soil column [2].

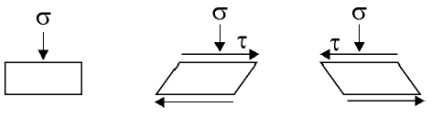

Figure 2.2 : Idealized stress condition for element of soil during an earthquake [2].

Seed and Idriss (1971) suggested a simplified procedure to assess liquefaction potential in soils since it has been the most referred approach for evaluating soil liquefaction. Intensity and the duration of cyclic loading are also considerable factors that have a significant influence on liquefaction in addition to soil properties. But first, it is essential to understand relationship between accelerations and shear stresses which a soil column is exposed to during cyclic loading. Basic approach, similar to the explanation of Equation 2.1, was the consideration of rigid body behavior of the soil column above a soil element at depth z [16]. However, as the soil column behaves as a deform-able body, the maximum shear stress at depth z, should be less than indicated in the basic approach and might be reduced by implying sort of stress reduction factor (r_d). Figure 2.3 below shows the determination of maximum shear stress in a soil column.

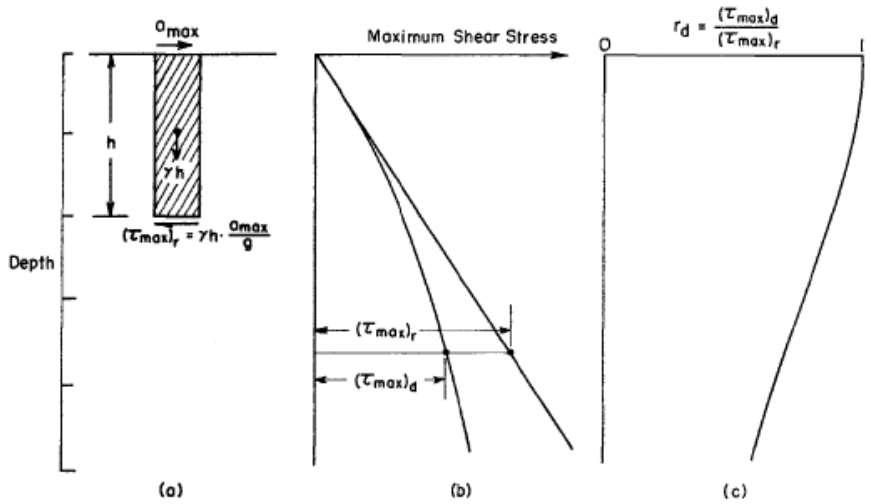

Figure 2.3 : Determination of maximum shear stress [16].

It has always been an important issue in liquefaction literature to determine r_d values dependent to depth z. Even there is a range of values for reduction factor in terms of different soil properties, according to Liao and Whitman (1986); equations 2.2 and 2.3 below may be used to estimate average values of stress reduction factor practically [17].

$$r_d = 1.0 - 0.00765z \quad \text{for} \quad z \leq 9.15m \tag{2.2}$$

$$r_d = 1.174 - 0.0267z \quad \text{for} \quad 9.15m < z \leq 23m \tag{2.3}$$

Moreover, the approximated mean value curve of r_d was expressed in reference to range for different soil profiles given in Seed and Idriss (1971) as [18];

$$r_d = \frac{1.0 - 0.4113z^{0.5} + 0.04052z + 0.001753z^{1.5}}{1.0 - 0.4177z^{0.5} + 0.05729z - 0.006205z^{1.5} + 0.001210z^2} \tag{2.4}$$

In addition, some other different stress reduction factor equations by implementing additional parameters like M_W (moment magnitude of an earthquake), V_s (shear wave velocity) [19, 20] have been expressed in the literature.

Figure 2.4 shows an example of time history of shear stresses during an earthquake [16]. It is seen that the actual time history of acceleration during an earthquake will have an irregular form so it is necessary to determine an average *equivalent* uniform shear stress, τ_a. Seed and Idriss (1971) suggested that the average equivalent shear stress is about %65 of the maximum shear stress based on a test data with a reasonable degree of accuracy.

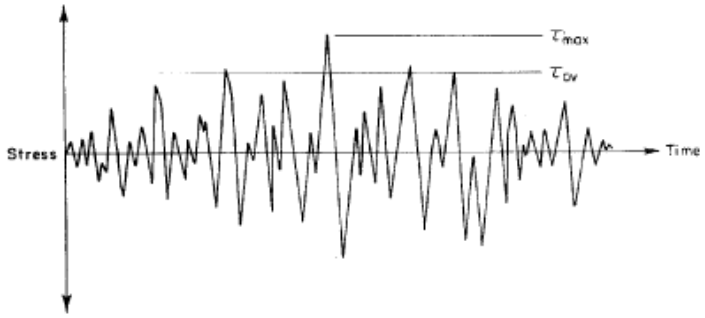

Figure 2.4 : Time history of shear stresses during an earthquake [16].

Regarding to these results, using the expression for τ_{max} in the Equation 2.1, the average equivalent uniform shear stress on a soil column during a cyclic motion can be written as;

$$\tau_a = 0.65 \frac{\gamma_t z}{g} a_{max} r_d \tag{2.5}$$

The simplified *"stress based"* method for assessing the earthquake induced liquefaction is basically derived from Newton's second low as discussed above.
Seed and Idriss (1971) also expressed the factor of safety (FS) against earthquake induced liquefaction triggering defined as;

$$FS = \frac{CRR}{CSR} \tag{2.6}$$

where CSR is a measure of the earthquake loading in terms of cyclic shear stress and CRR is a measure of the soil resistance determined by field or laboratory tests. While a_{max} is the horizontal component of the peak ground acceleration at the site, CSR is expressed as;

$$CSR = (\frac{\tau_{av}}{\sigma'_{v0}}) = 0.65\frac{a_{max}}{g}\frac{\sigma_{v0}}{\sigma'_{v0}}r_d \tag{2.7}$$

This definition had a great influence on further earthquake induced liquefaction potential assessment studies. As a result, calculation or estimation of two variables is required to assess liquefaction resistance of soils namely CSR and CRR. A detailed approach to identify liquefaction potential of saturated sand deposits requires cyclic tests however, the major challenge here is the limited capability of obtaining undisturbed specimens to be analyzed in the laboratory. Because of this incapability of obtaining undisturbed soil specimen for laboratory tests, more empirical approach based *in-situ* penetration test results gained popularity among engineers and researchers [21]. Youd *et al* (2001) noted that, "four *in situ* testing methods have now reached a level of sufficient maturity to represent viable tools for this purpose." These mentioned *in situ* test are standard penetration test (SPT), cone penetration test (CPT), shear wave velocity measurements (V_s) and the Becker penetration test (BPT).
In light of above discussed and explained approaches for evaluating liquefaction potential induced by earthquakes, in the following section SPT based liquefaction triggering procedures will be explained, considering SPT is the oldest and the still the most widely used and studied *in situ* test for liquefaction potential assessments. Furthermore, results of the model suggested in this thesis to evaluate liquefaction potential will be compared to SPT based assessment results in the succeeding chapters.

2.1.1 SPT Based Liquefaction Potential Assessment

Penetration test is one of the most broadly used test for soil investigations. Basics of this test cover driving a standardized penetrometer into the ground to estimate the soil resistance. Engineers use the method by correlating blow counts with various soil properties, in general. Figure below shows an illustration of a standard penetrometer [2].

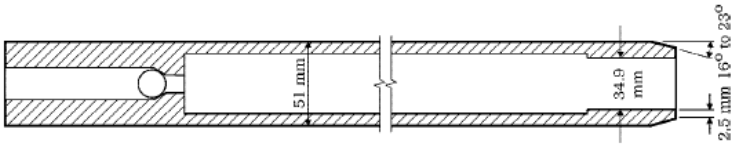

Figure 2.5 : Schematic illustration of the standard penetrometer. [2].

Sumer (2007) noted that "Basically the penetrometer is pushed into the ground below the bottom of a bore hole to a depth of $\frac{1}{2}$ ft (15cm) by means of the drop-hammer. Then the number of blow to drive the penetrometer 1 ft (30cm) is recorded" (p. 420). Several factors have also influence on SPT results and Table 2.2 below summarizes corrections to standard penetration test.

Table 2.2 : Corrections to SPT [18].

Factor	Equipment Variable	Term	Correction
Overburden pressure	–	C_N	$(P_a/\sigma'_{v0})^{0.5}$
Overburden pressure	–	C_N	$C_N \leq 1.7$
Energy ratio	Donut	C_E	0.5-1.0
Energy ratio	Safety	C_E	0.7-1.2
Energy ratio	Automatic Donut	C_E	0.8-1.3
Borehole diameter	65-115 mm	C_B	1.0
Borehole diameter	150 mm	C_B	1.05
Borehole diameter	200 mm	C_B	1.15
Rod length	$<$ 3 m	C_R	0.75
Rod length	3-4 m	C_R	0.8
Rod length	4-6 m	C_R	0.85
Rod length	6-10 m	C_R	0.95
Rod length	10-30 m	C_R	1.0
Sampling method	Standard	C_S	1.0
sampling method	without liners	C_S	1.1-1.3

Equation 2.8 combines these corrections where N_m is the measured standard penetration resistance; C_N is the factor to normalize measured standard penetration resistance to a common reference effective over-burden stress; C_E is the correction

factor for hammer energy ratio (ER), C_B is the correction factor for bore-hole diameter, C_R is the correction factor for rod length and C_S is the correction factor for sampling method [18].

$$(N_1)_{60} = N_m C_N C_E C_B C_R C_S \tag{2.8}$$

Seed and Idriss (1982) suggested an overburden stress correction factor due to increment in SPT N-values with increasing overburden stress. P_a is a reference pressure of $100kN/m^2$, and σ'_{v0} is the vertical effective stress [17].

In geotechnical engineering, using specially prepared charts where the quantity $(\frac{\tau}{\sigma'_0})$, CSR in other words, is plotted against corrected SPT blow counts is one of the most popular methods to evaluate liquefaction potential for earthquake induced liquefaction [2]. As the criteria for evaluation of liquefaction resistance based on SPT blow counts have been robust over years here Figure 2.6 shows CSR versus corrected SPT blow counts, $(N_1)_{60}$ [22].

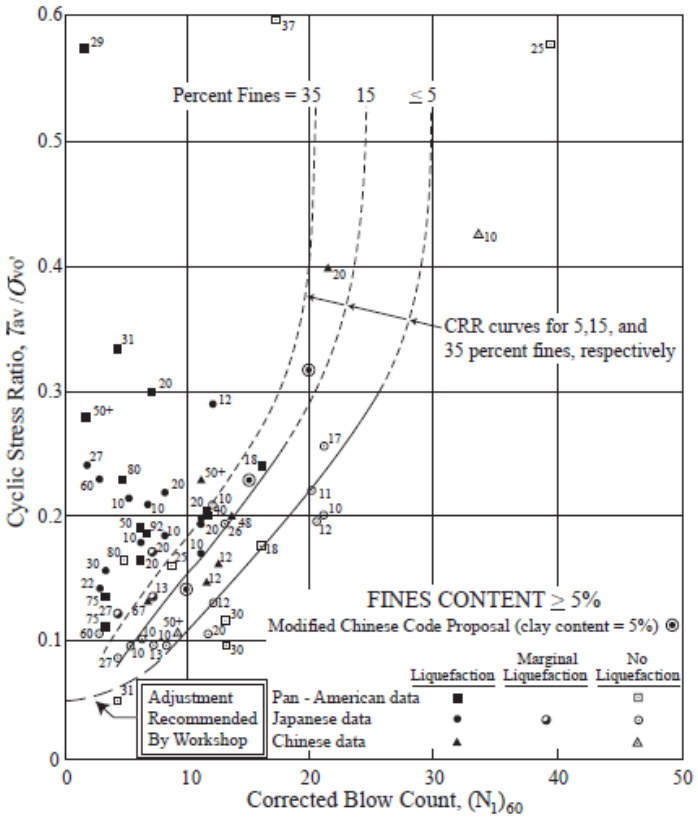

Figure 2.6 : Simplified base curve recommended for calculation of CRR from SPT data along with empirical liquefaction data [22].

Above figure shows calculated CSR and $(N_1)_{60}$ data from sites where liquefaction was observed or not during the past earthquakes. Moreover, CRR curves plotted over the chart to separate data for liquefaction and nonliquefaction incidents for various fine contents. Remember that given CRR curves are only valid for magnitude (M_W) 7.5 earthquakes yet scaling factors to adjust CRR curves for other magnitudes will be discussed later.

The CRR curve for fines contents of %5 is referred to "SPT clean-sand based curve" and an approximation for this curve can be made by following Equation 2.9.

$$CRR_{7.5} = \frac{1}{34-(N_1)_{60}} + \frac{(N_1)_{60}}{135} + \frac{50}{[10(N_1)_{60}+45]^2} - \frac{1}{200} \tag{2.9}$$

Equation 2.9 is also only valid for $(N_1)_{60} < 30$ where beyond these condition, clean granular soils are too dense to liquify [18]. An apparent increase of CRR with increased fines content is noted where this increment in the liquefaction resistance is not clear [23]. Based on the available site data Seed *et al* (1985) developed CRR curves for various fines content seen in the Figure 2.6. Below equation, given with related coefficients is used for correction of $(N_1)_{60}$ to an equivalent clean sand value $(N_1)_{60cs}$;

$$(N_1)_{60cs} = \alpha + \beta(N_1)_{60} \tag{2.10}$$

As an example, $\alpha = 5.0$ and $\beta = 1.2$ are used to plot CRR curves for soils contain more than %35 fines.

There are also various expressions of magnitude scaling factors (MSF) to reproduce the clean-sand base curve (CRR) while Equation 2.9 is only valid for earthquakes have magnitude of 7.5. The magnitude scaling factor (MSF) is used to account for duration effects on the triggering of liquefaction. Essentially these magnitude scalling factors shift the base curve upward or downward as shown in the figure 2.7.

MSF is highly recommended to use with some other correction factors such as, correction factor for high over-burden stresses K_σ and correction factor for static shear stresses K_α in practice. To assess earthquake induced liquefaction potential with SPT based tests one is also necessary to take the influence of age deposit in consideration [18]. Correction factors stated in this paragraph is not given in detail

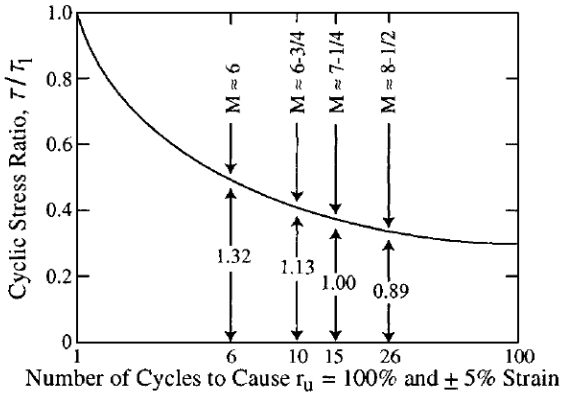

Figure 2.7 : Representative relationship between CSR and number of cycles to cause liquefaction given with different MSFs [12].

as a consequence of the scope of this thesis, however it is essential to mention.

SPT based liquefaction potential assessment procedure and used approaches are summarized above in this section in order to give general information. Further chapters will also refer SPT based evaluation for earthquake induced liquefaction potential where the relative density of the soil D_r, a significant parameter to investigate liquefaction potential, will be estimated.

2.2 Wave Induced Liquefaction

Marine soils are constantly exposed to wave action and the liquefaction phenomenon is generally associated with larger waves. These waves may have a period of 5 to 15 seconds, likewise wave heights up to 10-20 meters in the offshore locations [2]. Seabed soil may undergo liquefaction under waves where the effective stress between the individual grains disappear since the water-sediment mixture acts like a fluid with catastrophic consequences. There are two types of seabed seabed liquefaction namely momentary liquefaction and residual liquefaction [10]. Residual liquefaction is generated by buildup of pore pressure under progressive waves since momentary liquefaction is caused by an upward-oriented vertical pressure gradient in the soil during the passage of a wave trough [2]. The theoretical and experimental investigation of the build-up pore pressure and the resulting liquefaction of sediments under waves have been studied and reviewed extensively and substantial amount of knowledge has been gained on the buildup pore pressure and liquefaction. Each liquefaction mechanism under waves will be discussed separately while the pore pressure buildup within "*residual liquefaction*" will be given in detail since the method subjected in this

thesis covers a novel modeling approach for the onset of earthquake-induced sea bed liquefaction via an advance validated numerical model which is concerned only with residual liquefaction [10].

2.2.1 Momentary Liquefaction

Momentary liquefaction which occurs during the passage of the wave trough, is related to phase-resolved component of the waves. Under the wave trough the pore pressure (in excess of the hydro-static pressure) is negative (middle section of Figure 2.9). In the case of fully saturated soil, the pressure gradient is not very large however in the unsaturated soil condition the pressure gradient can be very large especially for small depths under the sea floor (Figure 2.8).

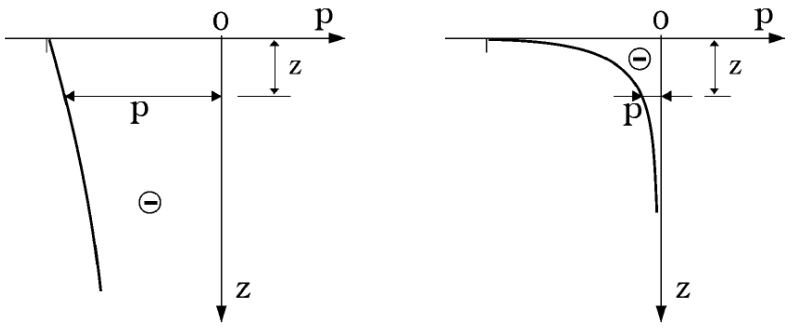

Figure 2.8 : Typical distributions of pore pressure (in excess of hydro-static pressure) during the passage of a wave trough. Saturated soil (*left*), Unsaturated soil (*right*) [2].

This pressure gradient is resulted in the generation of a small substantial amount of a lift at the top layer of the soil during the passage of the wave trough. When the lifting force overcomes the weight of the soil, the soil will fail and as a result it will be liquefied. This type of liquefaction is called *the momentary liquefaction*. it is necessary here to note that the term "*momentary*" is widely used in the literature to define this type of liquefaction as it can only survive in a very short period of time during the passage of the wave trough; for the rest of the wave period, the soil will be in the non-liquefied state.

Momentary liquefaction and resulting failures have widely placed in the literature. Sakai reported an extensive series of laboratory experiments and technical notes on the subsidence of concrete armor blocks gradually settled into the sandy sea floor in

Japan due to the decrease of the vertical effective stress in the sand bed and resultant liquefaction under wave action [24].

2.2.2 Residual Liquefaction

Sumer (2007) affirmed that the residual liquefaction will be best described by reference to a progressive wave over a horizontal sea floor (p. 6). The sea floor, in the presence of a progressive wave, will undergo periodic pressure variations resulting elastic shear deformations as shown in the Figure 2.9. Sea bed pressure increases under the wave crest hence the pressure that is occurred under the wave trough decreased due to expansion of the soil. This process proceed with a nearly 180 °phase difference between the soil and the water surface elevation which is resulted in generation of shear stresses in the soil (bottom part of Figure 2.9).

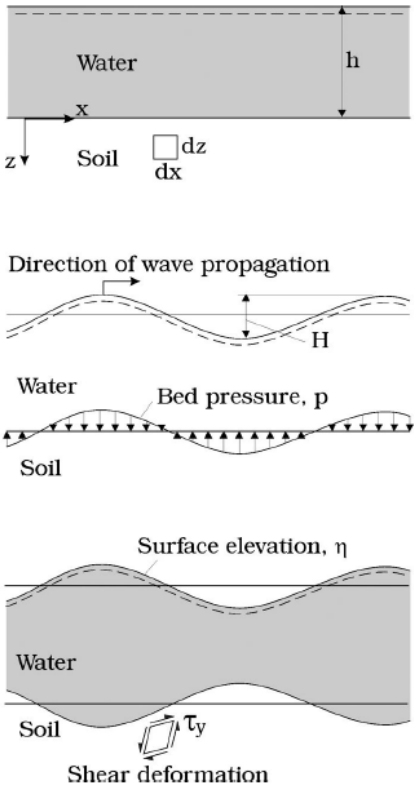

Figure 2.9 : Elastic deformation of the seabed soil under progressive wave [2].

If the grains are packed loosely, the cyclic shear stresses together with accompanying shear deformations in the sea bed will gradually rearrange the soil grains at the expense of the pore volume of the soil. In the case of an undrained soil conditions (water has an inability or quite limited ability to be drained, e.g. presence of silty material) while wave action continues the pore water pressure will continue to accumulate as well. As

it was mentioned before in the Section 1, when the accumulated pore pressure reaches such a level that exceeds initial effective stresses liquefaction occurs. Sumer and Cheng (1999) developed an analytical solution for the differential equation which governs the buildup pore pressure. In 1994 Hsu and Jeng produced an analytical solution for the latter quantity, solving the Biot Equations. The validated numerical model [10] that was used to calculate pore pressure buildup to estimate the earthquake-induced liquefaction susceptibility n the scope of this thesis essentially combines Sumer & Cheng's (1999) solution for the buildup pore pressure and Hsu & Jeng's (1994) solution for the shear stress in the soil.

Many studies created substantial amount of knowledge of the pore pressure buildup of pore pressure and the resulting liquefaction of sediments under waves (e.g. Seed & Rahman, 1978; Clukey *et al.*, 1983; Barends & Calle, 1985; Spierenburg, 1987; McDougal *et al.* 1989; de Groot *et al.*, 1991; de Groot & Meijers, 1992; Tzang *et al.*, 1992; Foda & Tzang, 1994; Foda, 1995; Sekiguchi *et al.*, 1995; Tzang, 1998; Sassa & Sekiguchi, 1999; Sumer *et al.* 1999; and the review given in Sumer & Fredsøe, 2002) [25].

3. METHOD

While earthquakes and waves both produce cyclic shear stresses (and accordingly cyclic shear deformations) in the seabed, the ones induced by earthquakes are more severe compared to that caused by waves. The method used in this study basically covers the comparison of the results obtained from a series of 1-D numerical model runs with the estimated ones from recent SPT based earthquake-induced liquefaction susceptibility assessment procedures. To make this comparison and predict the earthquake-induced seabed liquefaction an experimentally-validated mathematical model was modified, adapted and subsequently used to calculate pore pressure buildup within soil. Pore pressure buildup within "*residual liquefaction*" will be given in detail since the adapted and modified mathematical model concerns this type of liquefaction mechanism.

3.1 The Mathematical Model

In this study; an experimentally-validated mathematical model -also mentioned in previous sections- which was originally developed for wave induced liquefaction, was modified and adapted to predict earthquake-induced seabed liquefaction potential.
Wave induced residual liquefaction occurs in stages, since with the presence of propagating waves, pore water pressure builds up and this process is followed by *liquefaction* during which internal waves are experienced at the interface of the water body and the liquefied soil. After the liquefaction sequence, compaction develops due to dissipation of the accumulated pore water pressure and that stage finally results in formation of bed ripples (Figure 3.1) [25] .

In the second stage where the pore water pressure builds up, and eventually reach a maximum value, liquefaction starts. This study concerns this stage while the adapted mathematical model is also concerned with this initial sequence [10] too. The mathematical model consist of five components namely; equation for accumulated pore water pressure, the source term, number of cycles to cause liquefaction, the shear

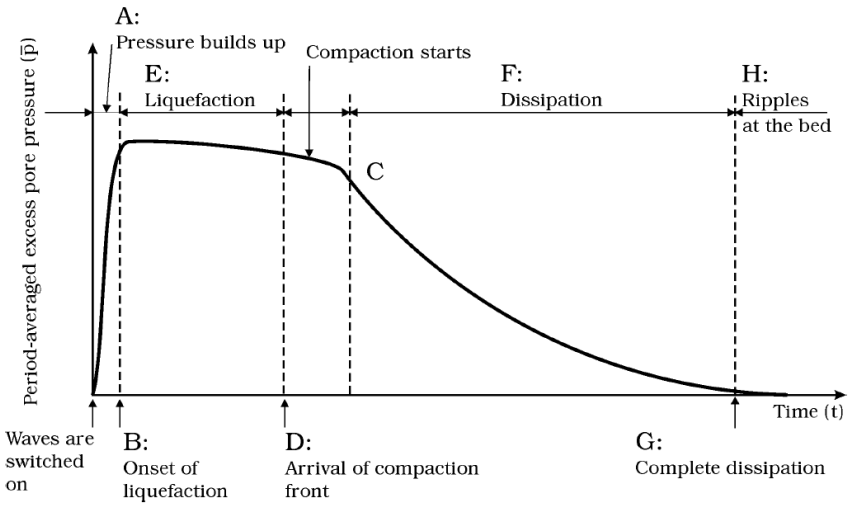

Figure 3.1 : Schematic desription of $\bar{p}$ as function of time.

stress generated in soil by wave and lastly the solution for the accumulated pore water pressure [10]. In this study shear stresses generated by earthquakes are taken into consideration by implementing a shear based approach given in section 2.1 so, four of these elements except "shear stresses generated in the soil by wave action" will be explained in the following sections.

Before explaining the components of the mathematical model it is necessary to mention Peacock & Seed's experiment which is one of the key elements of the theory behind the pore pressure buildup. In order to simulate the pore-pressure accumulation during an earthquake, Peacock and Seed (1968) conducted laboratory experiments under cyclic stress conditions causing liquefaction of saturated sand in *undrained* simple shear tests [2]. Sumer (2012), underlined the highlights of this noteworthy work and the conclusion of this study which will be summarized in consecutive paragraphs.

A simple shear box and and an arrangement was used in Peacock & Seed's tests and the soil sample was *consolidated* under an initial confining pressure which is distributed to soil and the water. Figure 3.2 the top plot shows the time series of the pore pressure, the middle plot shows shear strain time series and the bottom plot shows shear stresses time series. Cyclic shear stresses on the soil creates excess pore pressure ($\bar{p}$) and this pore pressure builds up as cyclic loading continues yet this whole process is similar as in the case of wave-induced liquefaction. Accumulated pore pressure (p) reaches such a level that exceed initial effective stresses (σ_0') and soil liquefies. As it is seen in the middle section of the Figure 3.2 the time when pore water pressure exceeded the initial

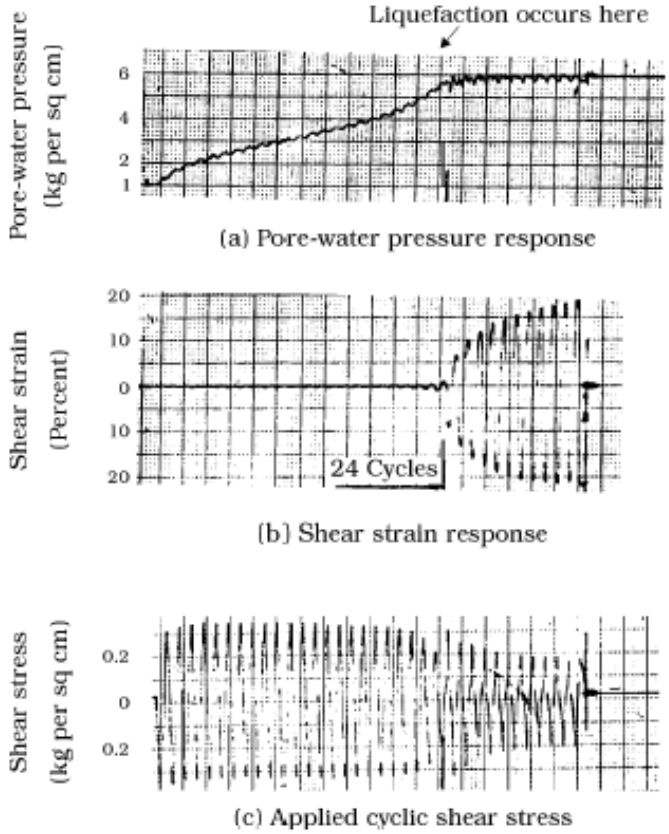

Figure 3.2 : Time series of pore pressure (*a*), shear strain (*b*), and shear stress in Peacock and Seed's (1968) experiment [2].

effective stresses was actually after 24th loading cycle was reached. What concluded in Peacock & Seed's experiment is; for the generation of the buildup of pore water pressure, water must have an inability or a very limited ability to be drained. If the water can drain from the soil, the pore pressure will be relieved resulting no buildup of pore water pressure.

3.1.1 Equation for Accumulated Pressure

Pore water pressure in the soil builds up as waves progress, identical to Peacock & Seed's experiment. Figure 3.3 shows time series of the pore pressure measured within the soil and water surface elevation together to illustrate the accumulation of the pore pressure [2]. The measurements were obtained in a wave flume with a silt bottom exposed to a progressive wave.

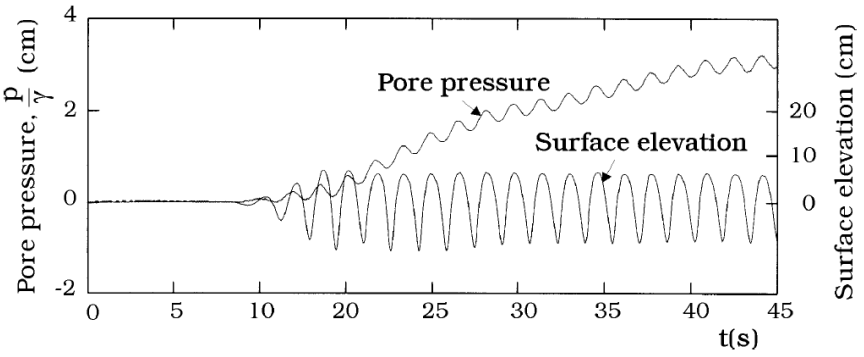

Figure 3.3 : Time series of excess pore pressure and surface elevation in Sumer *et al.*'s experiment [26].

Pore pressure is governed by the equations of equilibrium for poro-elastic soil (Biot consolidation equations, Equation 3.1).

$$G\bigtriangledown^2 u + \frac{G}{1-2\nu}\frac{\partial \varepsilon}{\partial x} = \frac{\partial p}{\partial x} \tag{3.1a}$$

$$G\bigtriangledown^2 v + \frac{G}{1-2\nu}\frac{\partial \varepsilon}{\partial y} = \frac{\partial p}{\partial y} \tag{3.1b}$$

$$G\bigtriangledown^2 w + \frac{G}{1-2\nu}\frac{\partial \varepsilon}{\partial z} = \frac{\partial p}{\partial z} \tag{3.1c}$$

$$\frac{k}{\gamma}\bigtriangledown^2 p = \frac{n}{K'}\frac{\partial p}{\partial t} + \frac{\partial \varepsilon}{\partial t} \tag{3.1d}$$

By considering the interested present process occurs in 2-Dimension, variations with respect to x is negligible. Since Equation 3.1 becomes shown below (Equation 3.2) for the present case.

$$G\frac{2-2\nu}{1-2\nu}\frac{\partial^2 w}{\partial z^2} = \frac{\partial p}{\partial z} \tag{3.2a}$$

$$\frac{k}{\gamma}\frac{\partial^2 p}{\partial z^2} = \frac{n}{K'}\frac{\partial p}{\partial t} + \frac{\partial^2 w}{\partial z \partial t} \tag{3.2b}$$

Differentiating the Equation 3.2a with respect to t, and the Equation 3.2b with respect to z, below Equation 3.3 is obtained where c_v is the *coefficient of consolidation*.

$$c_v \frac{\partial^3 p}{\partial z^3} = \frac{\partial^2 p}{\partial z \partial t} \tag{3.3}$$

$$c_v = \frac{Gk}{\gamma} \frac{2-2\nu}{(1-2\nu)+(2-2\nu)\frac{nG}{K'}} \tag{3.4}$$

Finally by integrating the Equation 3.3 with respect to z:

$$\frac{\partial p}{\partial t} = c_v \frac{\partial^2 p}{\partial z^2} + c \tag{3.5}$$

Above Equation 3.5 is obtained where c is the integration constant. The mathematical model is interested in the period-averaged excess pressure ($\bar{p}$) since the accumulated period-averaged pore water pressure is given below (Equation 3.6).

$$\bar{p} = \frac{1}{T} \int_t^{t+T} p dt \tag{3.6}$$

By substituting the term p in the Equation 3.5 with the period-averaged excess pressure ($\bar{p}$) below Equation 3.7 is obtained.

$$\frac{\partial \bar{p}}{\partial t} = c_v \frac{\partial^2 \bar{p}}{\partial z^2} + f \tag{3.7}$$

In Equation 3.7 the term f is the *source term* and represents the total amount of pore pressure generated per unit time and unit volume of soil where voids are included. In conclusion the Equation 3.7 is the emph governing equation for the buildup of pore pressure. the pore pressure is created through the term f and spreads out in the soil according to a diffusion process where c_v is the coefficient of consolidation, plays the role of familiar diffusion coefficient [2].

3.1.2 Source Term

The pore pressure generation is occurred due to cyclic action of shear deformations in the sea floor. The source term "f" represents the total amount of pore water pressure generated per unit time and volume of the soil. The source term can be described linearly where σ_0' is the overburden pressure value, N_l is the number of cycles to cause liquefaction and T is the period of the action. The equation of source term represents essentially a linear mechanism [10].

$$f = \frac{\sigma_0'}{N_l T} \tag{3.8}$$

where σ_0' is the initial mean normal effective stress, defined as:

$$\sigma_0' = \gamma' z \frac{1+2k_0}{3} \tag{3.9}$$

in which γ' is the submerged specific weight of the soil, namely $\gamma' = \gamma_t - \gamma$ (where γ_t is the specific weight of the soil and k_0 is the lateral earth pressure coefficient).

3.1.3 Number of Cycles to Cause Liquefacton

An other important quantity to analyze of liquefaction sequences is the number of cycles (N_l) to cause liquefaction. This quantity can be written as the function of the following parameters where τ is the shear stress acting on the soil, σ_0' is the initial effective stress and D_r is the relative the soil defined by void ratio given below (Equation 3.10).

$$N_l = f(\tau, \sigma_0', D_r) \tag{3.10}$$

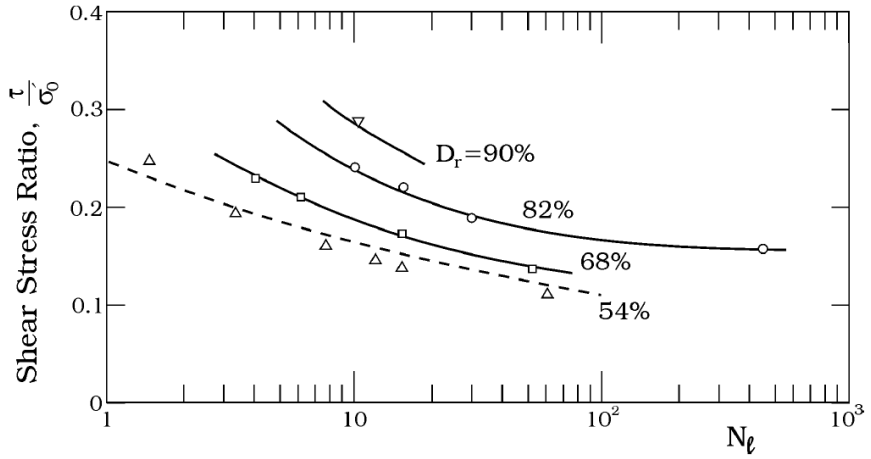

Figure 3.4 : Ratio of the amplitude of the shear stress in the soil to the initial effective stress vs. the number of cycles to cause liquefaction [2].

Sumer (2007) said that, "Peacock & Seed (1968) and Alba, Seed and Chan (1976) carried out undrained simple shear tests for different values of the relative density, and plotted the data N_l versus the normalized shear stress τ/σ_0' Figure 3.4 displays this diagram (adapted from Alba et al., 1976). It is seen that the number of cycles to cause

liquefaction increases tremendously with decreasing shear stress, and with increasing relative density, as expected." (p. 70).

The quantity N_l is modeled as it is given in the Equation

$$N_l = (\frac{1}{\alpha}\frac{\tau}{\sigma_0'})^{\frac{1}{\beta}} \tag{3.11}$$

where τ is the amplitude of the shear stress in the soil. Regarding the coefficients α and β in the Equation 3.11, these are mainly functions of the relative density of the soil (D_r) and calculated from the empirical expressions (Equation 3.12).

$$D_r = \frac{e_{max} - e}{e_{max} - e_{min}} \tag{3.12a}$$

$$\alpha = 0.34 D_r + 0.084 \tag{3.12b}$$

$$\beta = 0.37 D_r - 0.46 \tag{3.12c}$$

3.1.4 Solution to the Equation of Buildup Pore Water Pressure, Finite Soil Depth

The solution to Equation 3.7 for finite soil depth the source term f given within the Equation 3.8 and N_l given by Equation 3.10 is solved under the following initial and boundary conditions.

There is no accumulated in excess pore water pressure at the initial instance since;

$$t = 0, \bar{p} = 0 \tag{3.13}$$

At the mudline, the pore pressure continuously dissipates since;

$$z = 0, \bar{p} = 0 \tag{3.14}$$

Lastly for the case of an finite soil depth at the impermeable base (where $z = d$) the pressure "flux" should be zero.

$$z = d, \frac{\partial \bar{p}}{\partial z} = 0 \tag{3.15}$$

The solution of the pore water pressure buildup governing equation under above initial and boundary conditions are given as ([26]) :

$$\begin{aligned}\bar{p}(z,t) = \frac{2}{\pi}\sum_{m=1}^{\infty} sin\left[\left(m-\frac{1}{2}\right)\frac{\pi}{d}z\right]\int_{t'=0}^{tc_v(\frac{\pi}{d})^2} dt' \\ x\int_{\xi=0}^{\pi}\exp\left[-\frac{1}{4}(2m-1)^2\left[c_v\left(\frac{\pi}{d}\right)^2 t - t'\right]\right] \\ \sin\left[\left(m-\frac{1}{2}\right)\xi\right] g(\xi)d\xi\end{aligned} \tag{3.16}$$

in which $g(\xi)$ is

$$g(\xi) = \frac{1}{c_v}\left(\frac{d}{\pi}\right)^2\frac{1}{T}\gamma'\frac{1+2k_0}{3}\varepsilon\frac{d}{\pi}\left[\frac{1}{\alpha}\frac{3}{1+2k_0}\frac{\tau}{\gamma'\xi(d/\pi)}\right]^{\frac{-1}{\beta}} \tag{3.17}$$

with defined ξ by

$$\xi = \frac{z}{d/\pi} \tag{3.18}$$

Recall that τ in the Equation 3.17 is a function of the vertical distance z (or alternatively non-dimensional distance ξ in here) and the amplitude of the shear stress [10]. The original model above includes relatively sophisticated calculations to determine shear stresses (τ) under wave conditions. Here in this study; aforementioned "*stress based*" method given in previous sections (Equation 2.5) is used to calculate shear stresses caused by cyclic loading during earthquakes.

Instead of making complex calculations to determine shear stresses under cyclic loading according to the modeling method, the τ in the Equation 3.17 was substituted with the one calculated via basic "*stress based*" approach.

4. MODELING APPROACH

The fundamental of the numerical modeling approach studied for this thesis was mainly established over the detailed mathematical model and the method given in the previous section. The mathematical model, originally developed to estimate wave-induced liquefaction (actually calculates accumulation of pore water pressure under wave forces), was modified and adapted at first, then numerically solved under sort of cyclic loading (earthquake parameters) and environmental (soil properties) conditions to predict earthquake-induced liquefaction.

Study aimed to calculate the accumulated pore water pressure in a finite marine soil during an earthquake via adapted and modified model, and the time (t) and the depth (z) where period averaged pore water pressure ($\bar{p}$) exceeded initial mean effective stresses (σ'_0) were obtained from the model to obtain liquefaction time and the liquefaction depth in reference to given condition for the onset of liquefaction in Equation 4.1 ([2]).

$$\textit{liquefaction occurs when } \frac{\bar{p}}{\sigma'_0} > 1 \tag{4.1}$$

Numerical analysis was done under MATLAB® environment which is a powerful computing tool for iterative analysis and design processes with a programming language that expresses matrix and array mathematics directly. Solutions were made in the one-dimensional spatial domain where the liquefaction depth and the time was estimated.

At the beginning baseline values were determined for each soil and earthquake parameters. These values were also used in parametric model runs and model tests to validate and compare results with the CSR vs. SPT-N plots. Table 4.1 shows the determined earthquake baseline parameters and Table 4.2 shows the determined baseline parameters for the soil.

Table 4.1 : Earthquake and environment baseline parameters determined for the model tests

Parameter	Values
a (m/s^2), in terms of g)	0.01 0.02 0.035 0.05 0.07 0.1 0.15 0.20 0.25 0.35
T (Period, in seconds)	1
Earthquake duration, in seconds	30
g	9.81 m/s^2
h (water depth)	5 metres
ρ	1.02 t/m^3

Table 4.2 : Soil baseline parameters determined for model tests

Parameter	Value
K	1.9 10^6 kPa
s	2.60
ϕ'	36 °
k	$5x10^{-4}$ m/s
e_{min} (minimum void ratio)	0.4
e_{max} (maximum void ratio)	1
S_r (degree of saturation)	1
E	$25x10^3$ kPa
D_r	0.5
d (depth of liquefiable soil deposit)	5 metres

Apart from the parameters given in the tables above (Table 4.1 and Table 4.2) many other soil parameters (Table 4.3 were also taken into account in numerical modeling assessments. However these mentioned parameters are dependent to above given soil parameters. For example the *shear modulus of elasticity* of the soil deposit is dependent to the *modulus of elasticity* of soil deposit and the *Poisson's Ratio* which is also dependent to internal friction angle (ϕ').

Table 4.3 : Soil baseline parameters determined for model tests - 2

Parameter	Value
γ_w	specific weight of sea water (kN/m^3)
k_0	coefficient of lateral earth pressure
ν	Poisson's Ratio
n	Sediment porosity
γ'	Submerged bulk specific weight of the soil deposit (kN/m^3)
γ_t	Total unit weight of the soil deposit
G	Shear modulus of elasticity of the soil deposit (kPa)
K'	Volumetric modulus of elasticity of the soil deposit (kN/m^3)

Before comparing the numerical model solutions with the CSR-SPT N tables, corrected *SPT-N* values for corresponding relative densities (D_r) were needed to be

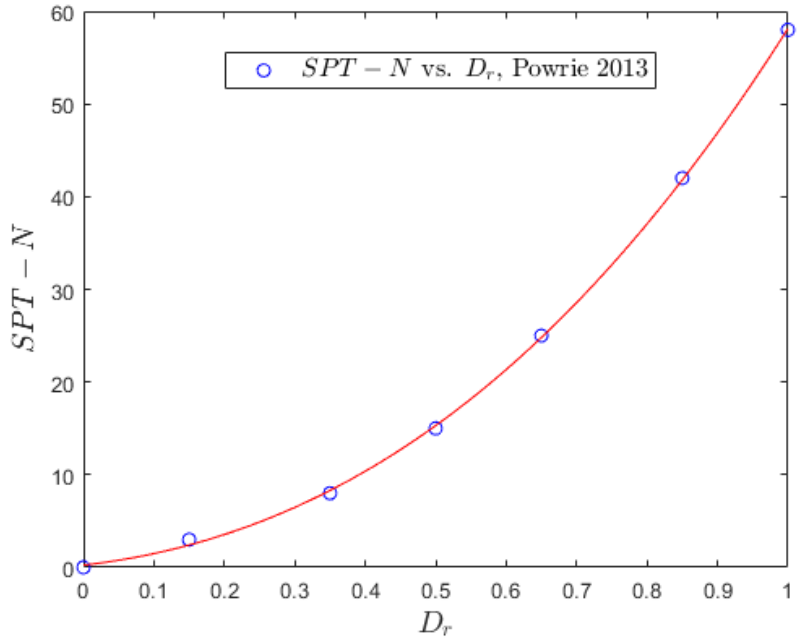

Figure 4.1 : Curve fitting between D_r and $SPT - N$ values

determined. With reference to Table 4.4. a 3rd order polynomial interpolation was used to fit a curve to determine corrected standard penetration blow counts (*SPT-N*) for corresponding D_r values which were used in model runs (Figure 4.1).

Table 4.4 : Correlation of density index I_D with corrected SPT blowcount $(N_1)_{60}$ ([27])

I_D	Classification	$(N_1)_{60}$
	Very loose	
0.15		3
	Loose	
0.35		8
0.5	Medium	13
0.65		25
	Dense	
0.85		42
	Very dense	
1		58

Table 4.5 below shows D_r values calculated using the fitted polynomial curve. These relative densities together with the corresponding SPT blow counts were also used in parametric model runs. Interpolation to define SPT-N blow counts was only done up to the value of "29" to achieve a good comparison hence according to CSR approach soils have a corrected blow counts higher than "30" are too dense to liquefy and accepted as *non-liquefiable*.

Table 4.5 : Model D_r values and corresponding corrected blow counts (SPT-N)

D_r	SPT-N
0.1	2
0.2	4
0.3	7
0.4	11
0.5	16
0.6	22
0.7	29

4.1 Model Calibration and Validation

In this section, model calibration and validation is discussed. There are two reasons behind comparing model results with the CSR-SPT N plots; first to validate the numerical model results for earthquake induced cyclic loading conditions since CSR tables present liquefaction status of the soil which were obtained during earthquakes by site measurements and second to calibrate the adapted numerical model results under cyclic stresses caused by earthquakes. As a validation and a calibration approach, numerical model tests were done both for different relative densities (D_r) and ground accelerations (a_g) together to compare results with the CSR vs. SPT-N plots. Calculated CSR values (τ/σ_0') for each soil and earthquake conditions were plotted together with the reference CRR (Cyclic Resistance Ratio) curve for fines content of %5 (Equation 2.9). The reference curve was suggested by A.F. Rauch in 1998 [18].

The Figure 4.2 covers model results for baseline soil and baseline earthquake parameters (Table 4.1 and Table 4.2). Cyclic stress ratios were calculated for different relative densities (Table 4.5) and plotted together with the reference CRR curve. The upper side of the reference CRR curve is known as the "liquefaction area" which is also widely used today by practitioners and engineers to determine liquefaction potential for the soils, where the CSR and corresponding SPT-N values belong to this area defines a liquefaction potential for the soil. Besides, blue circles in the scatter belong to a soil status which liquefaction occurred while red crosses belong to model results which where liquefaction did not occurred according to model calculations. At first sight the results seem satisfactory for lower values of SPT-N which are up to 15-16 blow counts (*loose sand*) however for higher relative densities -or corrected blow counts an

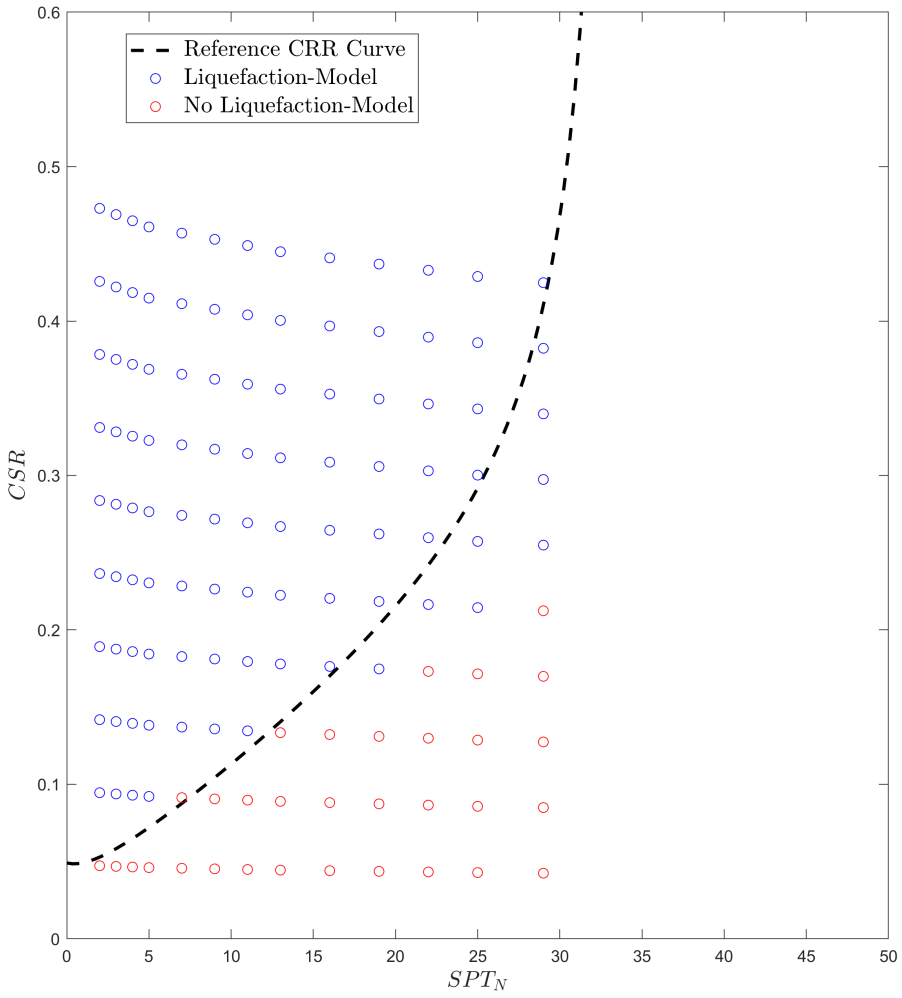

Figure 4.2 : Comparison of the model results with the reference CRR curve, (*baseline soil parameters "*$E = 25x10^3$*"*)

improvement of the numerical model might be needed. Although there is a lack of sampling in numbers for denser soils (soils have more than 20 SPT-N blow counts) model results with regard to higher relative densities barely indicates a calibration requirement and a necessity to review baseline soil parameters.

At this point the model sensitivity -which could answer models ability to estimate liquefaction potential for soils that have relatively higher relative densities (*medium dense to dense soil*) was investigated. Figure 4.3 is adapted from Sumer *et al.* 2012 basically illustrates how the wave-induced liquefaction model results are sensitive to modulus of elasticity of the soil (E). As it is seen in the Figure 4.3 pore pressure increases as Young's modulus of elasticity decreases. Sumer *et al.* 2012 also explained this behavior with the words "This is because the larger the value of E, the smaller

the cyclic elastic deformation caused by the wave, and thus the smaller pressure generated". Upon that, the value of the elasticity modulus to be used in model tests was discussed. The reason of this aforementioned inconsistency between the reference curve and the model results for relatively denser soils, is basically choosing the same modulus of elasticity value for all soil conditions. In fact, denser soils should have higher modulus of elasticity values.

Herein, sort of correlations between the modulus of elasticity (E) and relative densities were investigated to calibrate the adapted liquefaction model.

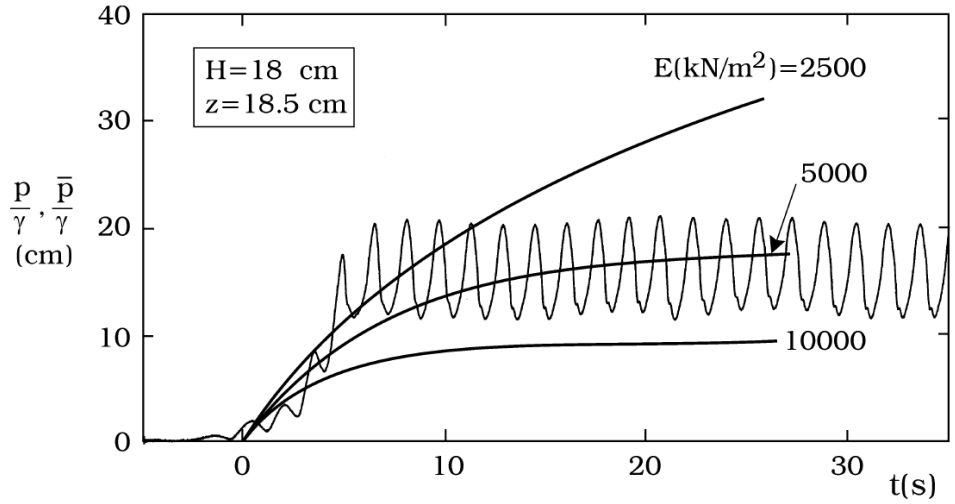

Figure 4.3 : Sensitivity of the numerical model, adapted from Sumer *et al.* 2012.

Even there are limited data for Young's modulus of elasticity of the soils in the literature, values of Young's modulus for sand vary in the range of $1x10^4$ to $2x10^5$ kN/m^2 [2] and Bowles [28] suggested correlations between modulus of elasticity and corrected SPT blow counts (Table 4.6). These correlations were evaluated in model calibrations.

Table 4.6 : Suggested correlation between corrected blow count and modulus of elasticity ([28])

Correlation No.	SPT-N versus Young's Modulus Correlation
E_1	$E = 500(N+15)$
E_2	$E = 7000\sqrt{N}$
E_3	$E = 6000N$

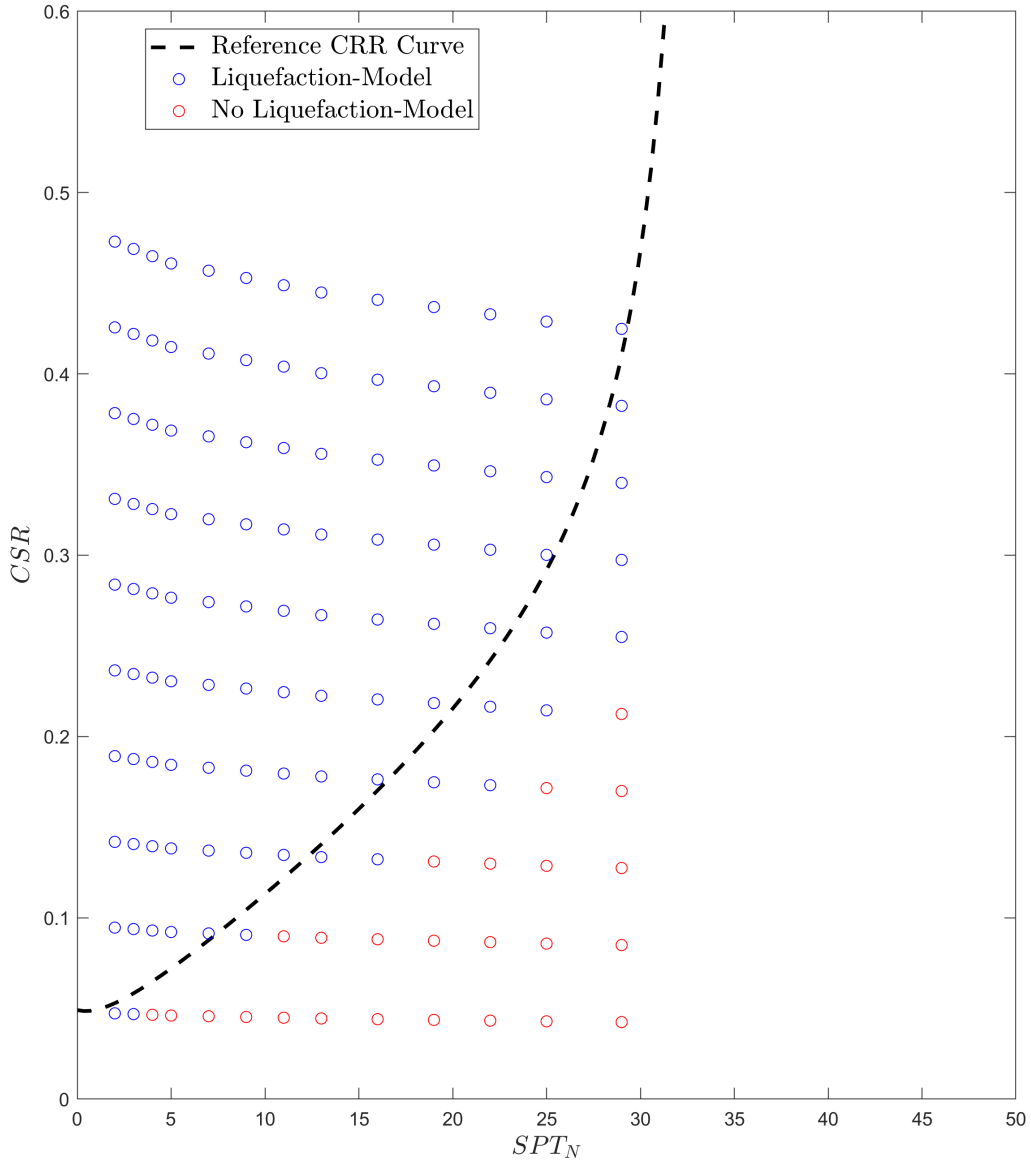

Figure 4.4 : Comparison of the model results with the reference CRR curve, E_1 correlation applied

Model test results after first equation of correlation E_1 was applied were shown in Figure 4.4. When the plot is compared with the first model runs serie ($E = 25x10^3$ *for all soil classifications*) it is seen that the prediction ability of the numerical model slightly changed in a negative way even for the loose soil conditions modeled. It was seen that, when the first correlation was applied, the value of the modulus of elasticity stays slightly out of the range of $1x10^4$ to $2x10^5$ for loose soils.

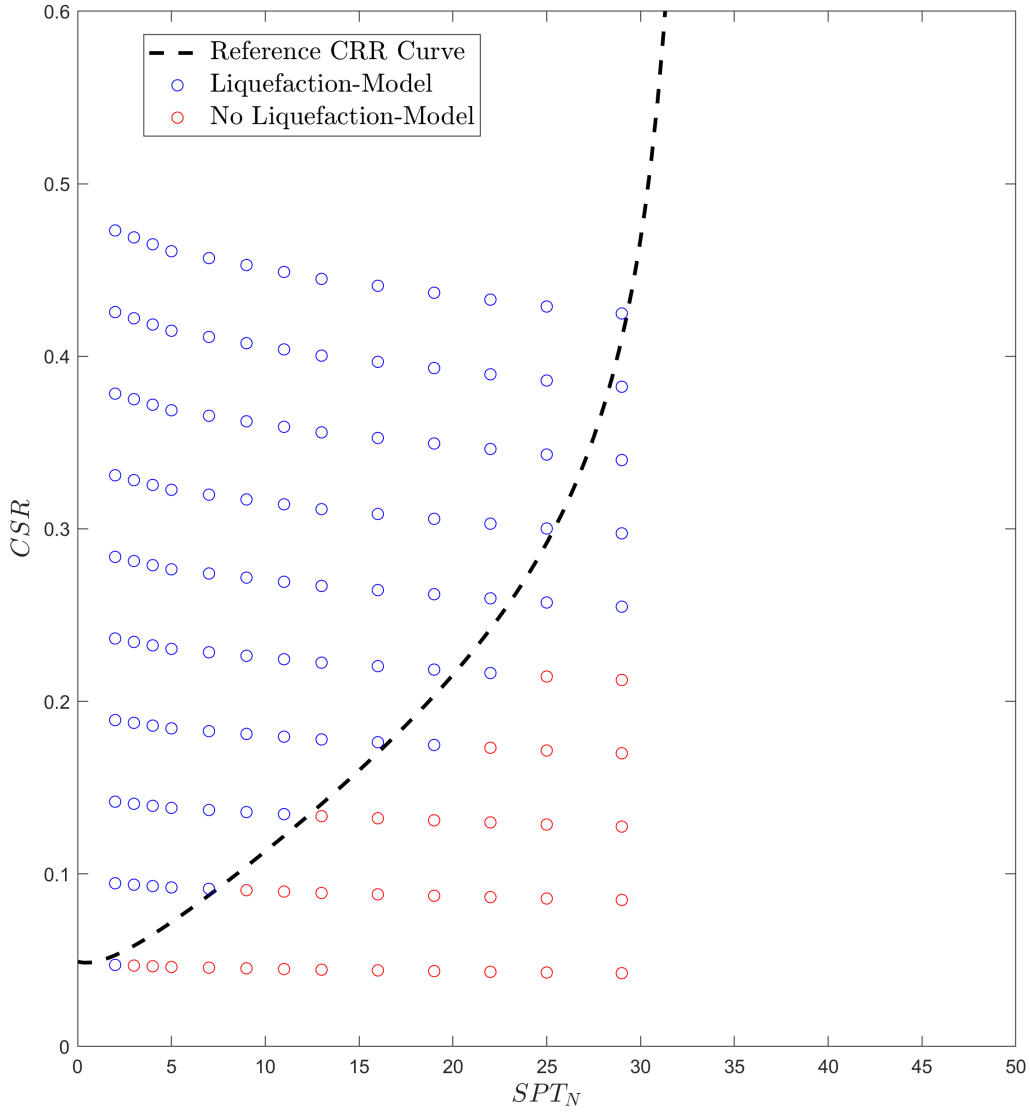

Figure 4.5 : Comparison of the model results with the reference CRR curve, E_2 correlation applied

Moreover, the second equation of correlation E_2 was used in model runs and the comparison of the results was given in the Figure 4.6. The results became satisfactory for loose soils however it was decided that the adapted model might need a better calibration especially for relatively denser soils which have corrected SPT blow counts of 20 or higher.

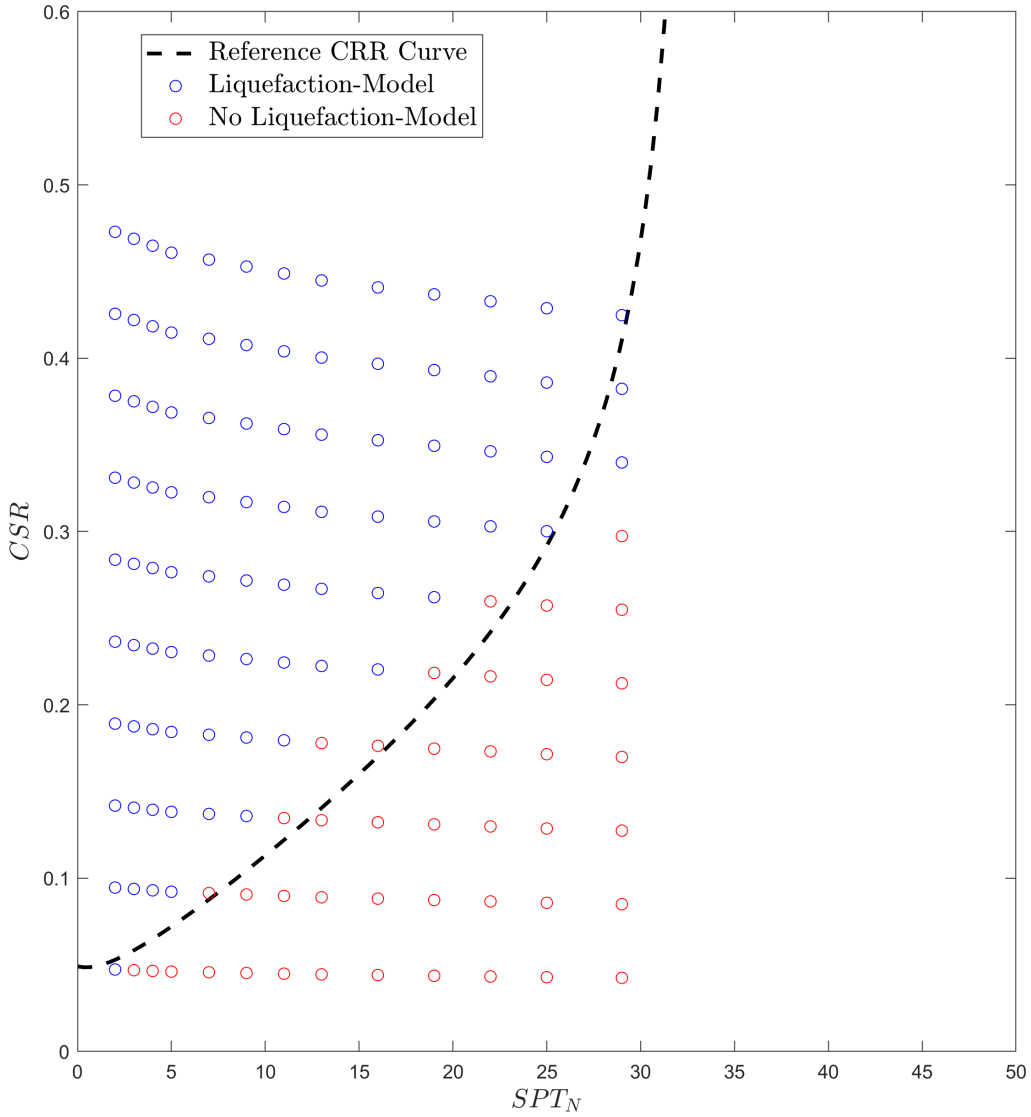

Figure 4.6 : Comparison of the model results with the reference CRR curve, E_3 correlation applied

Lastly, the third equation for the correlation was applied to adapted model for obtaining the Young's Modulus of the soils. At this time model results fitted better with the reference CRR curve for loose, medium dense and dense soils. Comparison in the plot was analyzed and it was seen that the adapted model barely creates more confident results by applying this correlation of $E = 6000N$ suggested by Bowles.

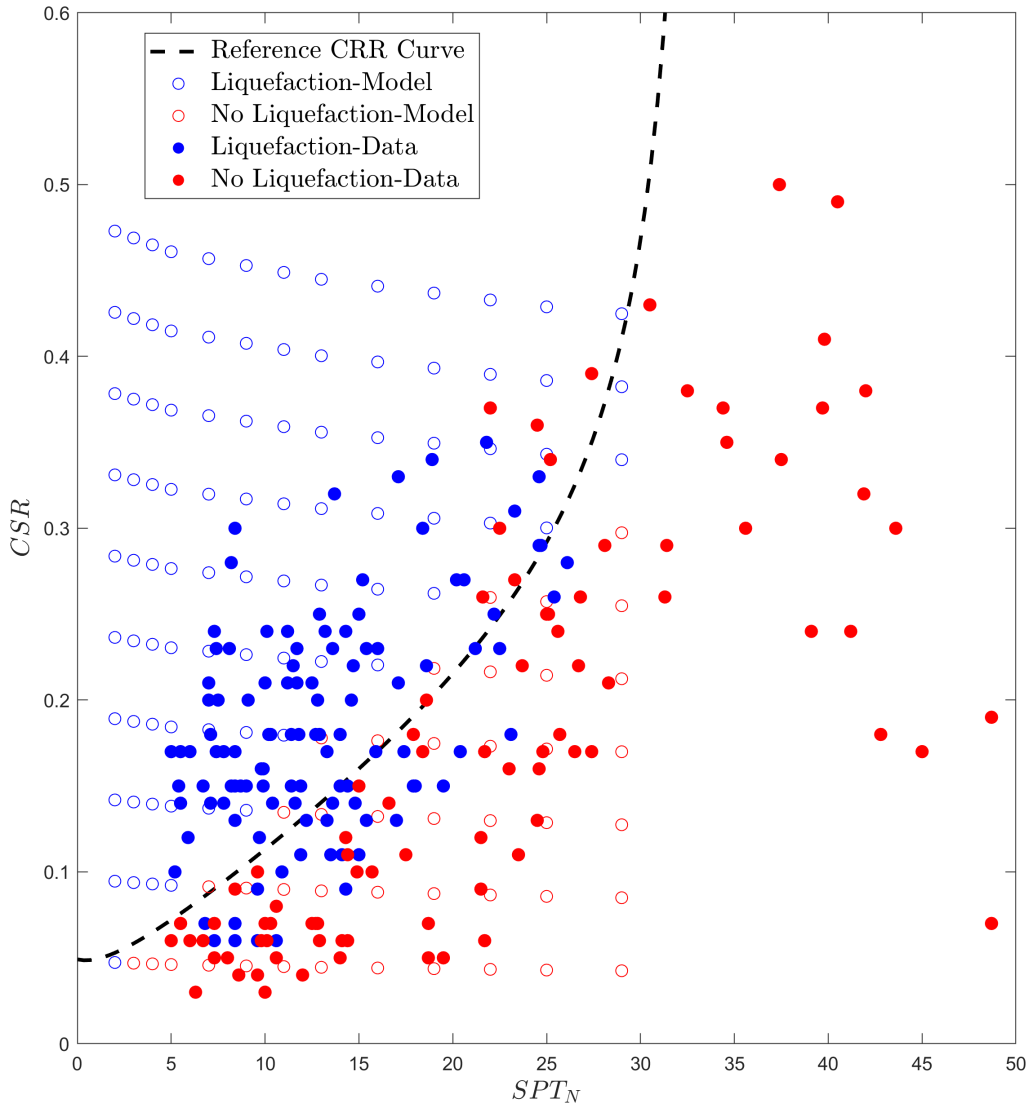

Figure 4.7 : Comparison of the model results with the historic site data

Beside comparing the results with the suggested reference cyclic resistance ratio (CRR) curve to calibrate the adapted model, a data set covering seismic liquefaction triggering and non-triggering case histories was also analyzed. This database is composed more than 200 liquefaction case histories for seismic events with moment magnitude values vary in the range of 5.9 to 8.3 [29]. Above figure contains each historic liquefaction cases and the model results. It is also seen in the figure that, calibrated model has the ability to estimate liquefaction or no-liquefaction status with a good accuracy in comparison with the historic site data.

4.2 Parametric Model Tests

A series of parametric runs also made to investigate and discuss the effect of different soil and earthquake parameters on the liquefaction. This parametric study was conducted to understand the numerical models abilities, sensitivity and responses under different conditions. Parametric model runs were made for different relative densities (D_r), hydraulic conductivities (k) and liquefiable soil deposit depths (d), ground accelerations (a_g), shaking periods (T). Except for the mentioned soil or earthquake parameters all other parameters stayed the same as they were summarized in Table 4.2 and Table4.1 (*baseline parameters*). Results of these parametric runs were discussed in the following sections.

4.2.1 Parametric Runs for Relative Densities, D_r

Relative density (D_r or I_D *density index*), which can be classified with standard penetration tests, has a significant role in liquefaction phenomena, is one of the key parameters in the adapted numerical model. As it was discussed in the previous section, relative density has a close relationship with the modulus of elasticity of the soil hence, it is harder for denser soils to liquefy if compared to looser soils, under the same cyclic loading conditions. When relative density of the soil increases, modulus of elasticity (E) of the soil increases too. A high modulus of elasticity means small cyclic shear deformations and this small values resulted in less pore water pressure generations within the soil. In conclusion, it is expected for denser soils -or soils have high relative densities- to have low liquefaction potential. It is also noted again in here; for the probabilistic CSR approach, soils have corrected blowcounts higher than 30 (*approx.* $D_r = 0.70$), are accepted as non-liquefiable soils.

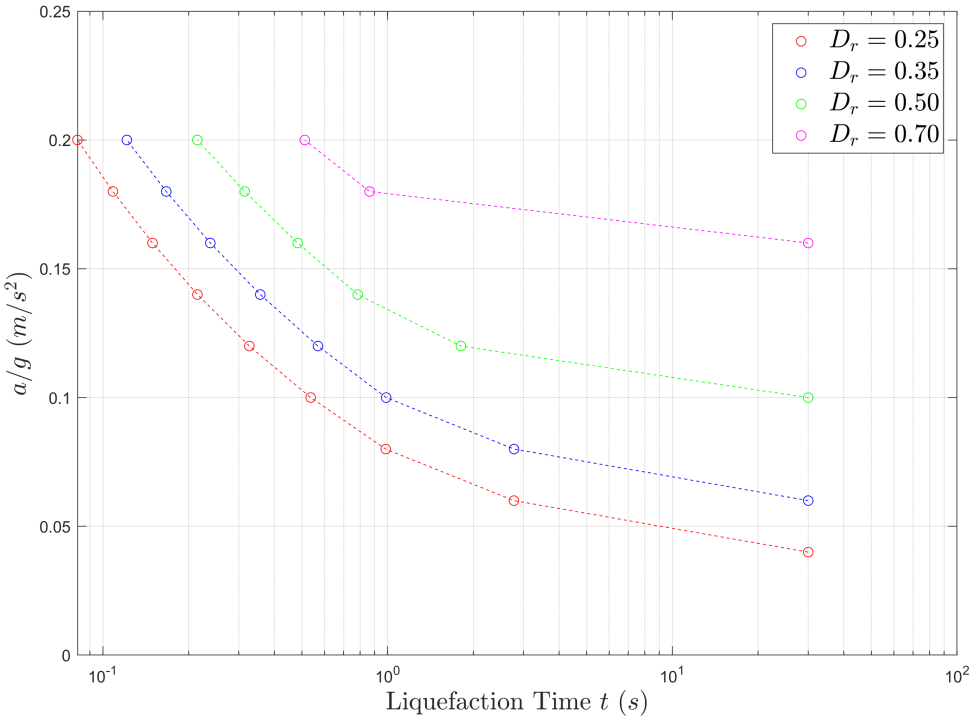

Figure 4.8 : Parametric run results for various relative density values

Figure 4.8 shows parametric model tests results conducted under baseline soil and earthquake conditions for different relative densities, $D_r = 0.25 - 0.35 - 0.50$ *and* 0.70 respectively. As the vertical axis shows a/g (*peak ground acceleration in terms of gravitational acceleration*), the horizontal axis shows t_L (*liquefaction time*) the time is needed for soil to liquefy. According to model results it is clearly seen that, denser soils need more time to reach the liquefaction state (Figure 4.8).

4.2.2 Parametric Runs for Hydraulic Conductivities, k

Hydraulic conductivity (k) basically defines soils water drainage ability. In case of undrained soil conditions, the condition refer to presence of soils that have inability or very limited-ability to drain water, as cyclic action continues the pore water pressure will continue to accumulate as well. when this accumulated pore water pressure reaches such a level that exceeds initial effective stresses, liquefaction occurs. Physical process behind the liquefaction phenomena closely related with the soil's water drainage ability, defined as the hydraulic conductivity.

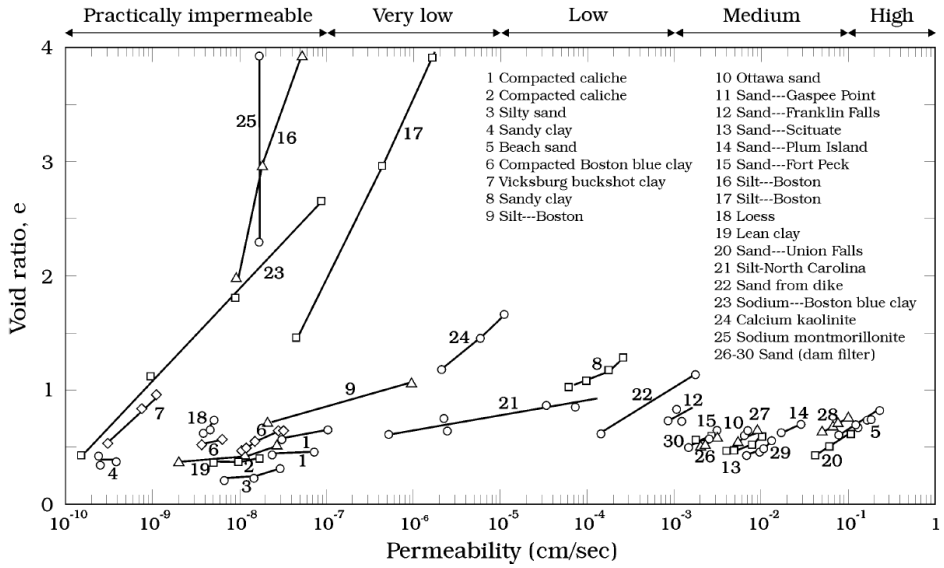

Figure 4.9 : Hydraulic conductivity values for various kind of soils, adapted from [2]

Figure 4.9 was adapted from Sumer 2014, summarizes the permeability value range of different soil types according to Lambe and Whitman, 1969. These test data were taken into consideration in parametric model runs since; the values of hydraulic conductivity (permeability, k) were selected from $5x10^{-5}\ cm/s$ to $1x10^{-3}\ cm/s$ correspond to soil classification of low permeability.

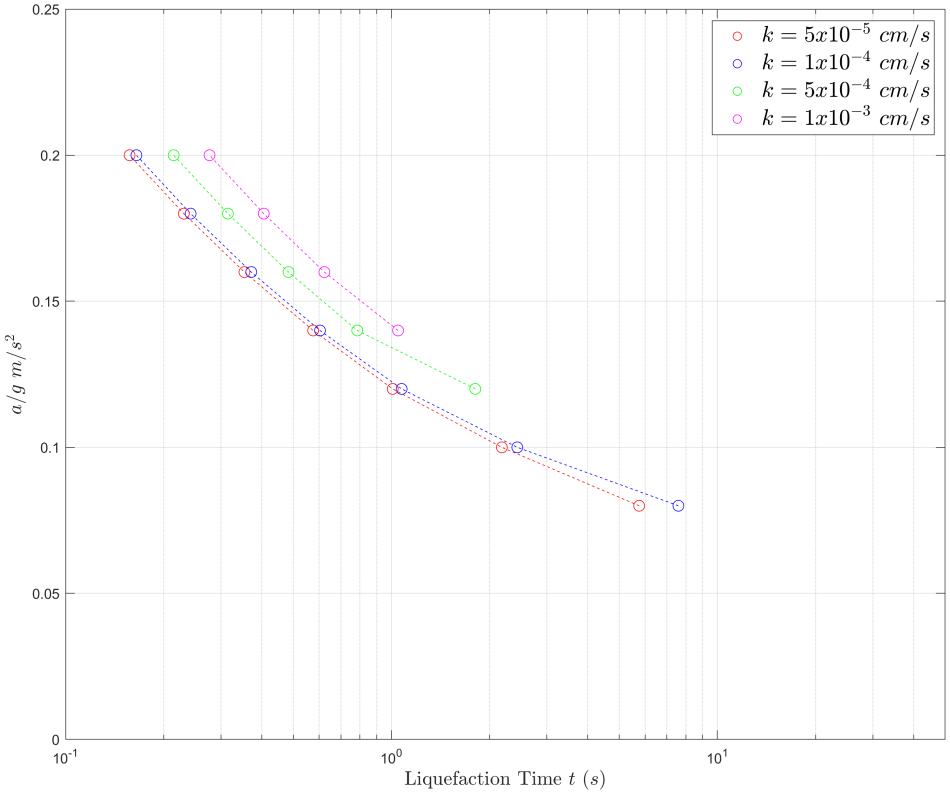

Figure 4.10 : Parametric run results for various permeability values

Even there is no significant difference under relatively higher ground accelerations, as permeability increases liquefaction potential decreases (Figure 4.10). Since liquefaction potential of a soil under cyclic conditions is correlated with the drainage ability of the soil, this results are also expected. Soil needs a capacity to hold the water content under cyclic loading conditions to be liquefied, because when the pore water pressure exceeds the initial effective stresses within the soil deposit, liquefaction occurs.

4.2.3 Parametric Runs for Liquefiable Soil Deposit Depths, d

Soil depth is an another parameter investigated with the parametric model runs. Soil depth here defines the thickness of the potentially liquefiable soil deposit. To investigate the effect of the soil deposit thickness a serie of parametric model runs were done for liquefiable soil depths of 5m, 10m, 15m and 20m respectively.

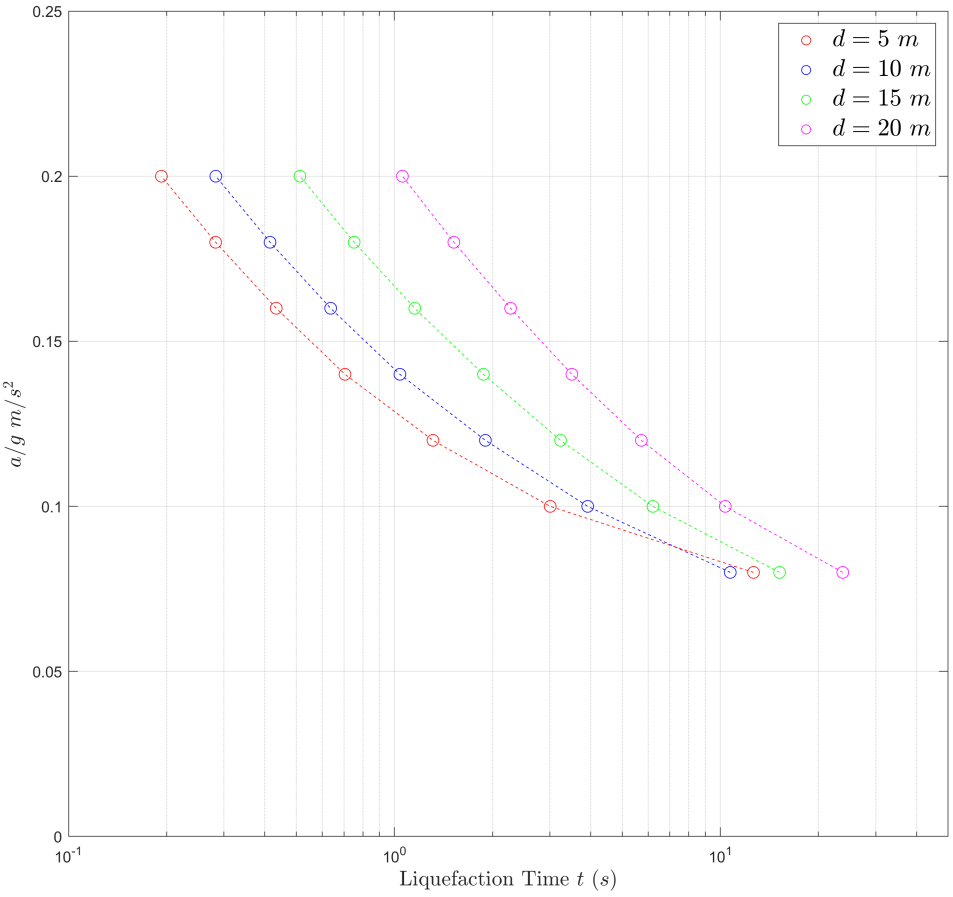

Figure 4.11 : Parametric run results for various liquefiable soil deposits

There is a notable difference between the model results conducted for relatively higher ground acceleration conditions, it was seen that as thickness of the liquefiable soil deposit increases, liquefaction time increases (Figure 4.11) noticeably. However for relatively lower peak ground accelerations, approximately between 0.05 and 0.10 g, this difference for the "liquefaction time" gets smaller.

4.2.4 Parametric Runs for Earthquake Motion Period, T

Influence of cyclic motion period (or frequency) was also investigated with parametric model runs regarding to various cyclic motion periods of 0.75 s, 1.00 s, 1.25 s, 1.50 s respectively. Since cyclic ground accelerations create cyclic shear stresses resulted in shear deformations in the soils, the period of the cyclic motion has an influence on liquefaction process.

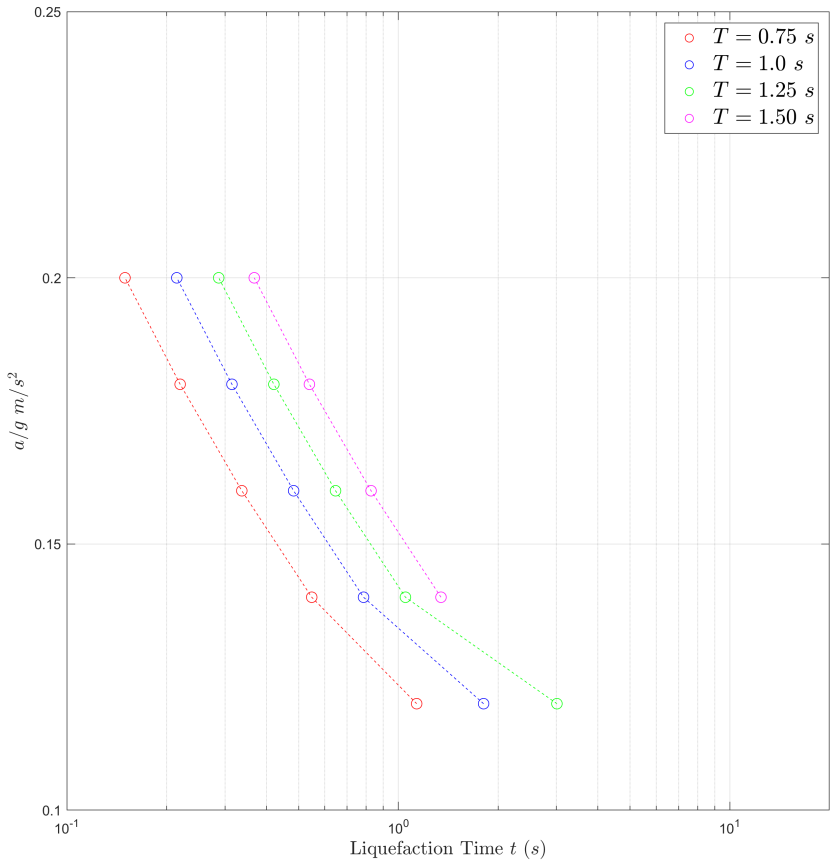

Figure 4.12 : Parametric run results for various cyclic motion periods

Due to parametric model results, cyclic motion period has a noticeable influence on liquefaction time. According to results, under high frequency cyclic motions soil

liquefies faster. Lower periods of cyclic motion basically pressurize water within the soil faster, as a result the soil liquefies faster (4.12).

4.2.5 Parametric Runs for Internal Friction Angle, ϕ

Parametric models runs were also conducted for different values of internal friction angles (ϕ) of 34°, 36°, 38°and 40°respectively.

According to results of the parametric runs to investigate the influence of internal friction angle on liquefaction, it is seen that soils have a higher internal friction angle liquefies faster (Figure 4.13).

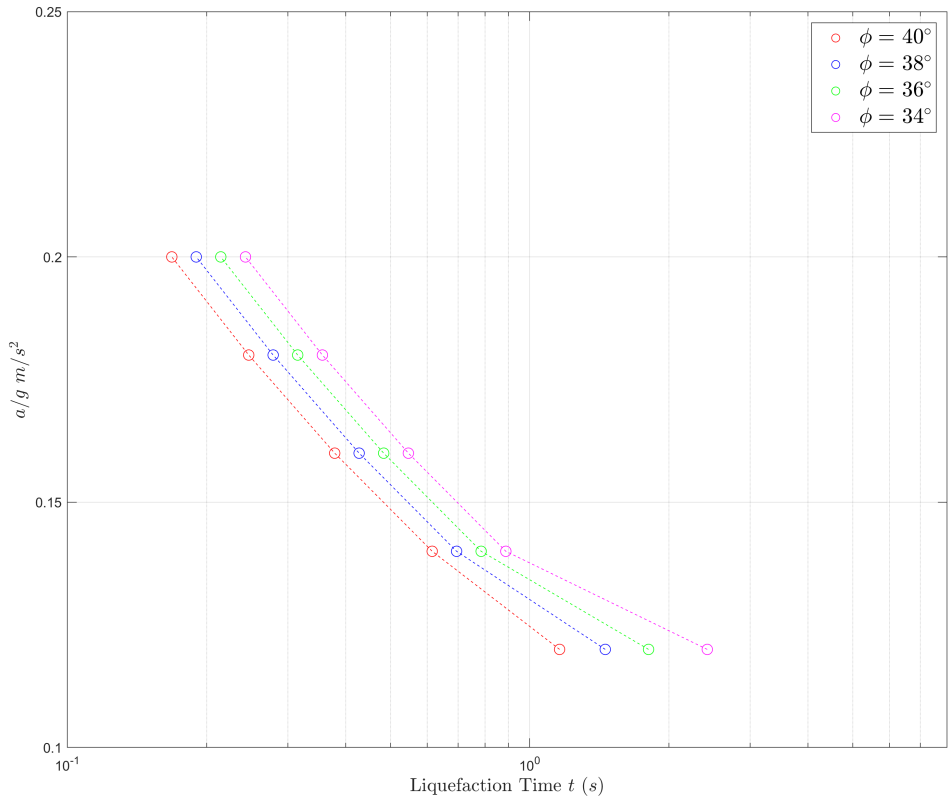

Figure 4.13 : Parametric run results for various angle of internal friction ϕ

5. RESULTS AND DISCUSSIONS

In this study an experimentally validated mathematical model which was originally developed to estimate liquefaction under cyclic wave action was adapted and modified to predict earthquake induced seabed liquefaction potential of the seabed. First, it was determined to apply a simplified stress based method to determine shear stresses during cyclic ground motions created by earthquakes. These stresses were taken into account as shear stresses generated in the soil during an earthquake. Since shear stresses generated in the soils during cyclic motions creates cyclic deformations which cause liquefaction under sufficient soil and environmental conditions.

Under determined baseline earthquake and soil parameters, model tests were assessed and the results were compared with the widely used CSR/CRR tables. These approach is a widely used procedure to identify liquefaction of the soil by practitioners and engineers. The aim of this thesis is to create an alternative liquefaction assessment tool for practitioners by adapting a validated liquefaction model. Comparison of the model results and CSR/CRR tables was done by plotting the suggested reference cyclic resistance ratio (CRR) curve (for $M_W = 7.5$) over the model results. Comparing model results with the reference CRR curve also showed how the model was calibrated hence the CRR approach covers soil liquefaction status data obtained are gathered on site during earthquakes. During model calibration assessment, some suggested correlations between corrected standard penetration blow counts ($SPT - N$) between Young's modulus of elasticity (E) were evaluated and the correlation which fits model results to reference curve was chosen for the following parametric runs. By choosing an adequate correlation between SPT-N values and Young's modulus of elasticity model calibration was done. For a final assessment for the model calibration, a recent probabilistic and deterministic liquefaction susceptibility studies were also investigated. Model results were compared with extensive liquefaction site data for comparison, and models ability to estimate liquefaction potential was analyzed.

To understand models representation capabilities as well as influences of different type of soil and environment/earthquake parameters, series of parametric model runs were conducted. Parametric runs were done for different relative densities (D_r=0.25 - 0.35 - 0.50 - 0.70), permeability values (k= $5x10^{-5}$ cm/s, $1x10^{-4}$ cm/s, $5x10^{-4}$ cm/s and $1x10^{-3}$ cm/s), liquefiable soil deposit depths (d=5m, 10m, 15m and 20m), earthquake motion periods (T= 0.75 s, 1.00 s, 1.25 s and 1.50 s) and angle of internal frictions (ϕ= 34°, 36°, 38°, 40°).

According to model results it is clearly seen that, denser soils since they have higher modulus of elasticity values need more time to reach the liquefaction state due to small water pressure generations within the soil deposit. Even there is no significant difference under relatively higher ground accelerations, as permeability increases liquefaction potential decreases. There is also a notable difference recognized between the model results which were conducted for relatively higher ground acceleration conditions, it was seen that as thickness of the liquefiable soil deposit increases, liquefaction time increases. According to parametric model results, water within the soil pressurized faster under high cyclic action frequencies and the soils have a higher internal friction angle liquefies faster.

Beside parametric model runs to investigate models capabilities, with reference to calibration assessments; it is seen that the adapted numerical model has a satisfactory ability to predict earthquake-induced seabed liquefaction. This model could be an alternative tool to assess liquefaction susceptibility to be used by practitioners instead of or together with the recent probabilistic and deterministic liquefaction susceptibility assessment approaches.

REFERENCES

[1] (2001). *PIANC (2001): Seismic design guidelines for port structures. Working group no. 34 of the Maritime Navigation Commission.*, Lisse : A.A. Balkema Publishers, 2001.

[2] **Sumer, B.M.** (2014). *Liquefaction Around Marine Structures.*, Advanced Series on Ocean Engineering: volume 39, Singapore ; New Jersey : World Scientific, 2014.

[3] **Idriss, I.M. and Boulanger, R.W.** (2008). *Soil Liquefaction During Earthquakes*, Earthquake Engineering Research Institute.

[4] **Sawicki, A. and Mierczyński, J.** (2006). Developments in modeling liquefaction of granular soils, caused by cyclic loads, *Applied Mechanics Reviews*, *59*(2), 91 – 106.

[5] **T. Christian, J.**, **K. Taylor, P.**, **K.C. Yen, J. and R. Erali, D.** (1974). Large diameter underwater pipeline for nuclear power plant designed against soil liquefaction, *6th Offshore Technology Conference*, volume II.

[6] **Herbich, J.B.** (1984). *Seafloor scour: Design guidelines for ocean-founded structures*, volume 4, Marcel Dekker Incorporated.

[7] **Miyamoto, T.**, **Yoshinaga, S.**, **Soga, F.**, **Shimizu, K.**, **Kawamata, R. and Sato, M.** (1989). Seismic prospecting method applied to the detection of offshore breakwater units settling in the seabed, *Coastal Engineering in Japan*, *32*(1), 103–112.

[8] **C. Chaney, R. and Y. Fang, H.** (1991). Liquefaction in the coastal environment: An analysis of case histories, *10*, 343–370.

[9] **Young, Y.**, **White, J.**, **Xiao, H. and Borja, R.** (2009). Liquefaction potential of coastal slopes induced by solitary waves, *Acta Geotechnica*, *4*(1), 17–34.

[10] **Sumer, B.**, **Kirca, V.O. and Fredsoe, J.** (2012). Experimental validation of a mathematical model for seabed liquefaction under waves, *International Journal of Offshore and Polar Engineering*, *22*, 133–141.

[11] **B Seed, R.**, **Cetin, K.**, **ES Moss, R.**, **Kammerer, A.**, **Wu, J.**, **M Pestana, J.**, **Riemer, M.**, **Sancio, R.**, **D Bray, J. and Kayen, R.** (2003). Recent advances in soil liquefaction engineering: a unified and consistent framework.

[12] **Seed, H. and Idriss, I.** (1982). *Ground motions and soil liquefaction during earthquakes*, Engineering monographs on earthquake criteria, structural

design, and strong motion records, Earthquake Engineering Research Institute.

[13] **Andrews, D.C. and Martin, G.R.** (2000). Criteria for liquefaction of silty soils, *Proceedings, 12th World Conference on Earthquake Engineering*, NZ Soc. for EQ Engrg. Upper Hutt, New Zealand.

[14] **Boulanger, R.W. and Idriss, I.M.** (2004). *Evaluating the potential for liquefaction or cyclic failure of silts and clays*, Center for Geotechnical Modeling Davis, California.

[15] **Elnashai, A. and Di Sarno, L.** (2015). *Fundamentals of Earthquake Engineering: From Source to Fragility*, Wiley.

[16] **Seed, H.B. and Idriss, I.M.** (1971). Simplified procedure for evaluating soil liquefaction potential, *Journal of Soil Mechanics & Foundations Division*.

[17] **Liao, S.**, **Whitman, R. and of Technology. Department of Civil Engineering, M.I.** (1986). *A Catalog of Liquefaction and Non-liquefaction Occurrences During Earthquakes*, Department of Civil Engineering, MIT.

[18] **Youd, T.L. and Idriss, I.M.** (2001). Liquefaction Resistance of Soils: Summary Report from the 1996 NCEER and 1998 NCEER/NSF Workshops on Evaluation of Liquefaction Resistance of Soils, *Journal of Geotechnical and Geoenvironmental Engineering*, *127*(4), 297–313.

[19] **Idriss, I. and Boulanger, R.** (2006). Semi-empirical procedures for evaluating liquefaction potential during earthquakes, *Soil Dynamics and Earthquake Engineering*, *26*(2), 115 – 130, 11th International Conference on Soil Dynamics and Earthquake Engineering (ICSDEE): Part II.

[20] **Cetin, K.O.**, **Seed, R.B.**, **Kiureghian, A.D.**, **Tokimatsu, K.**, **Harder, L.F.**, **Kayen, R.E. and Moss, R.E.S.** (2004). Standard penetration test-based probabilistic and deterministic assessment of seismic soil liquefaction potential, *Journal of Geotechnical and Geoenvironmental Engineering*, *130*(12), 1314–1340.

[21] **Sumer, B.M.**, **Ansal, A.**, **Cetin, K.O.**, **Damgaard, J.**, **Gunbak, A.R.**, **Hansen, N.E.O.**, **Sawicki, A.**, **Synolakis, C.E.**, **Yalciner, A.C.**, **Yuksel, Y.** *et al.* (2007). Earthquake-induced liquefaction around marine structures, *Journal of Waterway Port Coastal and Ocean Engineering*, *133*(1), 55–82.

[22] **Robertson, P. and Fear, C.** (1996). Soil liquefaction and its evaluation based on SPT and CPT.

[23] **Seed, H.B.**, **Tokimatsu, K.**, **Harder, L.F. and Chung, R.M.** (1985). Influence of SPT procedures in soil liquefaction resistance evaluations, *Journal of Geotechnical Engineering*, *111*(12), 1425–1445.

[24] **Sakai, T.**, **Hatanaka, K. and Mase, H.** (1992). Wave-Induced effective stress in seabed and its momentary liquefaction, *Journal of Waterway Port Coastal and Ocean Engineering*, *118*.

[25] **Sumer, B.**, **Dixen, F.**, **Fredsoe, J. and Kaan Sumer, S.** (2006). The sequence of sediment behaviour during wave-induced liquefaction, *Sedimentology*, *53*, 611 – 629.

[26] **Sumer, B.M.**, **Cheng, N.S.** *et al.* (1999). A random-walk model for pore pressure accumulation in marine soils, *The Ninth International Offshore and Polar Engineering Conference*, International Society of Offshore and Polar Engineers.

[27] **Powrie, W.** (2013). *Soil Mechanics: Concepts and Applications*, CRC Press.

[28] **Bowles, J.** (1997). *Foundation Analysis and Design*, Civil engineering series, McGraw-Hill.

[29] **Cetin, K.O.**, **Seed, R.B.**, **Kayen, R.E.**, **Moss, R.E.**, **Bilge, H.T.**, **Ilgac, M. and Chowdhury, K.** (2018). Dataset on SPT-based seismic soil liquefaction, *Data in brief*, *20*, 544–548.

CURRICULUM VITAE

PHOTO

Name Surname: Giray Çıvak

Place and Date of Birth: Bursa 31.08.1987

E-Mail: giraycivak@gmail.com

EDUCATION:

- **B.Sc.:** 2014, Istanbul Technical University, Faculty of Civil Engineerig, Civil Engineering

PROFESSIONAL EXPERIENCE AND REWARDS:

- 2014 - 2015 Researcher, MERMAID Project, Istanbul Technical University
- 2015 - 2018 Civil Engineer, CEC Marine
- 2018 - to date Civil Engineer, Arti Proje

PUBLICATIONS, PRESENTATIONS AND PATENTS ON THE THESIS:

- Kirca, V.S.O., Civak, G., Sumer, B.M. "Deprem Kaynaklı Deniz Tabanı Sıvılaşması İçin Yeni Bir Model Yaklaşımı", 9. Ulusal Kıyı Mühendisliği Sempozyumu 1-3 Kasım, 2018, Adana, Türkiye.
- Kirca, V.S.O., Civak, G., Sumer, B.M. "A Novel Modelling Approach For Earthquake-Induced Seabed Liquefaction", International Conference on Coasts, Ports and MArine Structures (ICOPMAS), 26-28 November, 2018, Tehran, Iran.

OTHER PUBLICATIONS, PRESENTATIONS AND PATENTS:

- Kirca, V.S.O., Elginöz, N., Çıvak, G., Özkan, E., Baş, B., Kabdaşlı, M.S. "Avrupa Denizlerinde Çok Amaçlı Açık Deniz Platformlarının Bugünü ve Geleceği, MERMAID Projesi", 9. Ulusal Kıyı Mühendisliği Sempozyumu, Istanbul, 7-9 Kasım, 2014.
- Varol, Ö.E., Kirca, V.S.O., Çıvak, G., Kabdaşlı, M.S. "Aşma Tipi Bir Dalga Enerji Dönüştürücüsünün Performans Parametrelerinin İncelenmesi", 9. Ulusal Kıyı Mühendisliği Sempozyumu, Istanbul, 7-9 Kasım, 2014.